MASTER COPY SENT TO NTIS 1 NOV. 1971

PASSIVE GEODETIC SATELLITE

INFLATABLE SPHERE ASSEMBLIES

By S. J. Stenlund, C. A. Dahlgren, A. J. Wendt, D. Lingo, D. Roiseland, and T. J. Neuhaus

G. T. Schjeldahl Company
Northfield, Minnesota

Distribution of this report is provided in the interest of information exchange. Responsibility for the contents resides in the authors or organization that prepared it.

NATIONAL AERONAUTICS AND SPACE ADMINISTRATION

CONTENTS

CONTENTS

PASSIVE GEODETIC SATELLITE

INFLATABLE SPHERE ASSEMBLIES

By S. J. Stenlund, C. A. Dahlgren, A. J. Wendt, D. Lingo,
D. Roiseland, and T. J. Neuhaus
G. T. Schjeldahl Company

SUMMARY

The construction of the PAGEOS (Passive Geodetic Satellite) 30.48-meter-diameter inflatable sphere is described in detail, from design analysis, through design testing, manufacturing and inspection, to the final packing in a canister. An original method is derived for predicting the reliability of the sphere, without demonstration tests or predetermined component failure rates. The sphere was put in orbit from Vandenburg AFB on June 23, 1966.

INTRODUCTION

As a continuation of the NASA effort in support of the National Geodetic Satellite Program, an ECHO I type satellite was launched into a near-polar orbit 4,250 kilometers in altitude from Vandenburg AFB on June 23, 1966. The 30.48-meter-diameter aluminum-coated spherical satellite can be observed from the ground as a point source of light while it reflects the incident sunlight. Simultaneous photographs of this light source taken against the star background by two or more widely separated ground-based cameras will enable geodesists to determine the spatial coordinates of each camera position. An interconnected series of camera positions has been established to cover the entire surface of the earth, thereby permitting geometric determination of each camera position within a single reference system. The use of this satellite for geodetic purposes will continue for a 5-year minimum period during which the necessary photogrammetric observations will be made to provide, for the first time, a purely geometric determination of the shape and size of the earth.

This report describes the work in analysis, testing, and fabrication of the inflatable sphere assemblies required for the Passive Geodetic Satellite project.

DEFINITIONS

1. Gores - the shaped segments that are sealed together to form a sphere.

2. Gore blank - a length of full width material sufficient for cutting a gore and samples.

3. Splice tape - a narrow adhesive coated strip of material used to seal gores together.

4. Polar cap - circular disc of material bonded to gore ends.

5. Final seal - the last splice tape used to seal the first and last gore together.

6. Bond - the fastening force exerted by an adhesive-coated splice tape when activated by heat.

7. Butt joint seal - a joint of two gore edges held together with splice tape.

8. Bitape seal - a joint of two gore edges held together with a tape on both sides.

9. Vent hole - a reinforced hole (0.16 cm diameter) cut in the sphere to allow entrapped air to escape during packing and evacuation.

10. Equator - an imaginary circle around the center of the sphere, equally distant at all points from the polar caps.

11. North and South poles - the outermost points of a sphere corresponding to the centers of the polar caps.

12. Adhesion - the sticking together of PAGEOS material which is caused in part by the properties of the surfaces of the film. It is accelerated by heat and pressure as of the sealing wheel.

13. Seam creep - slippage of the splice tape adhesive which causes separation of a sealed joint during high stress and usually at elevated temperatures.

14. Accordion pleating - tapered longitudinal gore fold whose width determines the final package size on two sides. This is the first stage of sphere packaging.

15. Folding - the second stage of sphere packing, made in the transverse direction of the gore.

16. Zigzag fold - the method of folding in which the pleated stack is folded back and forth on itself so that unfolding can start at either end or both ends at once.

17. Pleated stack - the resulting symmetrical cigar-shaped pile of sphere material after the pleating operation is complete.

18. Folded stack - the resulting symmetrical pile of packaged sphere material after all packing steps are complete.

19. Evacuation sleeve - an air-tight plastic tube used to protect and enclose a pleated sphere; when evacuated, the sleeve forces entrapped air out of the sphere.

SYMBOLS

		Units
A	absorptivity	--
a	albedo of the earth	--
C	Celsius	degrees
C_S	solar constant	2.00 cal/cm^2 minute
c	arc	meters
D	diameter	meters
e	emissivity	--
f	function	--
h	altitude	kilometers
K	Kelvin	degrees
k	$r_E/(r_E + h)$	--
ℓ	perimeter of valve duct opening	meters
N	number of gores	--
P	loading tension	dynes
p	pressure	dynes/cm^2
Q	uniform loading	dynes/cm
r	radius	meters
S	stress	dynes/cm^2
T	temperature	degrees Celsius or Kelvin
t	thickness	millimeters
u	upper 90 per cent confidence limit of the difference of population means	various
X	distance from seal edge along sphere surface	centimeters
ε	strain	--
μ	population means	various
σ	Stefan Boltzmann constant	5.672×10^{-5} ergs/cm^2 sec ^{o}K

θ	half angle subtended by gore at equator	radians
ϕ	angle measured from the equator toward the pole of the sphere	radians

Subscripts:

cs	cold spot
E	earth
HS	hot spot
i	inner or inside
o	outer or outside
S	solar
s	seal
v	vapor

DESCRIPTION OF SATELLITE

The PAGEOS satellite was constructed from 0.0127-millimeter (0.5 mil) thick polyethylene terephthalate (PET) plastic film with approximately 2,200 angstroms of aluminum vapor deposited on the outside surface. The thin film of aluminum serves two purposes: first, it reflects sunlight, having a reflectance of 83 to 90 per cent and a specular component greater than 93 per cent, to wavelengths in the visible spectrum, and second, it protects the film from damaging ultraviolet radiation.

The aluminum was vapor deposited on long rolls of 137.16-centimeter-wide plastic film. From these rolls, 84 gores required for the construction of each inflatable sphere were cut into the required shape, sealed together with splice-plate tape, and capped at each polar end. The gores were approximately 113.99 centimeters wide at the equator and 47.85 meters long as seen in figure 1. These gores were butted together and sealed with a 2.54-centimeter-wide tape made from the same material as used for the gores with a thin layer of thermosetting resin applied to the plastic side of the film to serve as the adhesive. (See figure 1). The tape was applied to the inside surface of the sphere.

Other major components of the sphere, essential in maintaining the strength in the polar areas, are the end caps shown in figure 2. The end caps serve as termini for the tips of the gores. This is a practical method of bringing all the converging gore tips together, and transferring the circumferential stresses across the poles when the sphere is under pressure. As seen in figure 2, the polar end caps of a PAGEOS sphere have a ring of metallic conductive paint near the edge of the cap which electrically connects all the gores. These strips of metallic paint, applied under the polar cap, are called continuity rings. Figure 2 also shows that there are two layers of material in each polar end cap. The outer layer is the metalized PET, and the inner layer of 0.0254-mm thick, nonmetalized PET is the main load bearing

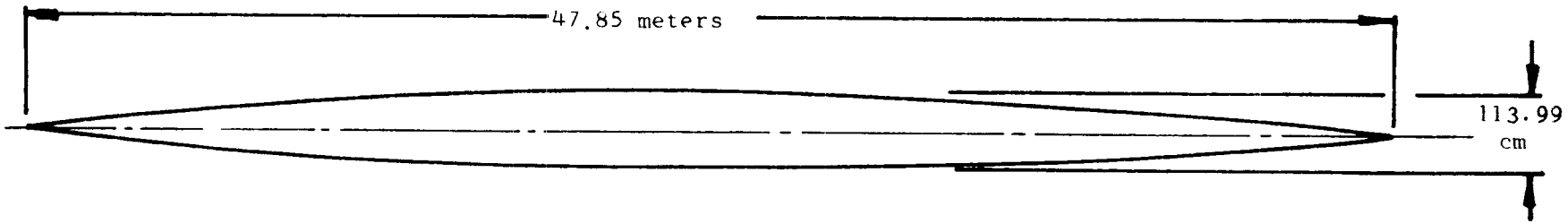

The gore width at any distance, $r\varphi$, from the equator is given by the formula

$$\frac{2\pi r}{N} \cos \varphi$$

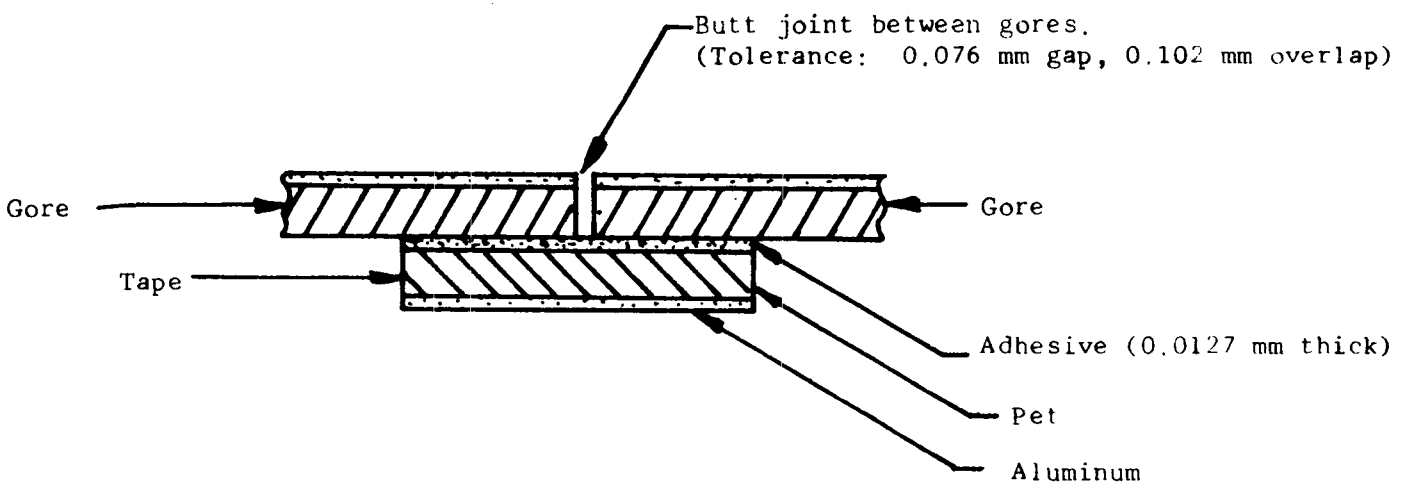

Figure 1.- Typical gore and gore seal.

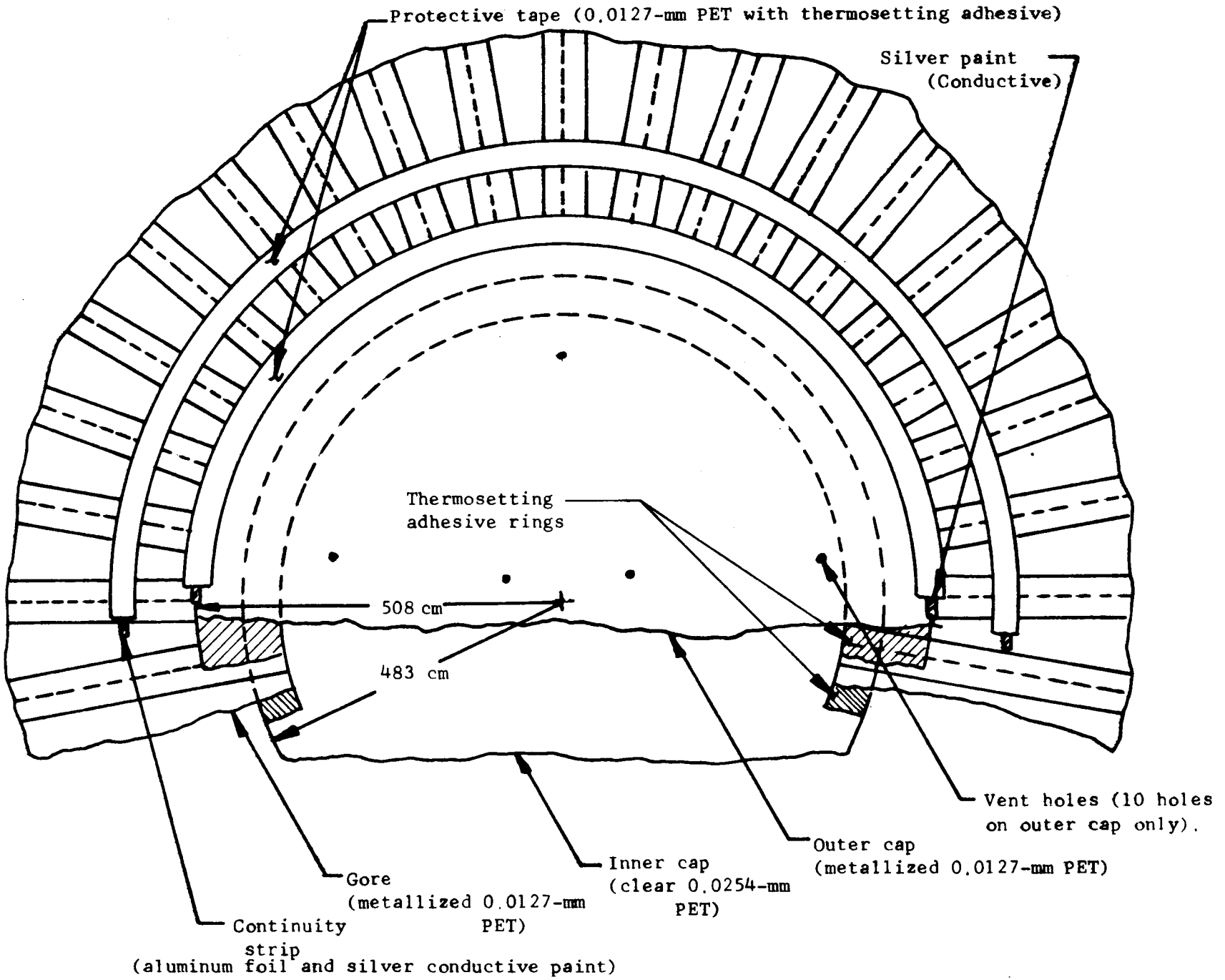
Protective tape (0.0127-mm PET with thermosetting adhesive)
Silver paint (Conductive)
Thermosetting adhesive rings
508 cm
483 cm
Vent holes (10 holes on outer cap only).
Outer cap (metallized 0.0127-mm PET)
Inner cap (clear 0.0254-mm PET)
Gore (metallized 0.0127-mm PET)
Continuity strip (aluminum foil and silver conductive paint)

material. The outer layer is primarily for continuity in the optical and thermal aspects of the sphere.

When a PAGEOS sphere is ready for delivery, it is complete with an inflation system. This system is a carefully weighed combination of powders (benzoic acid and anthraquinone) distributed on the inside of the gores prior to final closure of the sphere. The powder was dusted in each pleat during the pleating operation. A schematic of the completed sphere (figure 3) shows gore and end cap arrangement.

A full-scale sphere, 30.48 meters in diameter, is shown inflated in figure 4.

DESIGN ANALYSIS

Stress Analysis Flight Sphere

Assembling a sphere from flat panels yields a shape which has a circular cross-section through the poles, but is more or less polygonal through the equator. The degree of departure from a circle depends on the number of panels or gores used in the construction. For the PAGEOS sphere 84 gores were used.

If it is assumed that the joining tapes do not stretch, the 84-sided polygon can be made spherical by stretching the center of the gores.

Analysis for stress conditions in the PAGEOS flight sphere can be separated into areas consisting of the sphere body, tapes, and polar caps.

If the assumptions are made that (1) the sphere shape is initially a polygon, and (2) the tapes act as a constraint, the strain and stress required to attain the spherical shape can be determined as follows (see figure 5):

$$\varepsilon = \left[\frac{\theta}{\sin \theta} - 1 \right] , \qquad (1)$$

therefore

$$\varepsilon = \left[\frac{\pi/N}{\sin(\pi/N)} - 1 \right] \qquad (2)$$

Strain as a function of the number of gores has been plotted in figure 6. The graph shows that for N=84, a strain of 2.4×10^{-4} cm/cm is required to transform the polygonal shape to a spherical shape. Using Hooke's law, the corresponding stress may be calculated as 8.274×10^{6} dyn/cm^2. This figure indicates that the spherical shape will be attained at a very low internal pressure; however, if the spherical shape is to be maintained without internal pressure, the material must be stressed to obtain a permanent deformation equivalent to 2.4×10^{-4} cm/cm. Assuming Hooke's law applies, the stress required to attain the necessary permanent deformation may be determined by drawing a parallel to the initial straight line portion of the stress-strain curve for PET. This parallel must intersect the abscissa at 2.4×10^{-4} cm/cm.

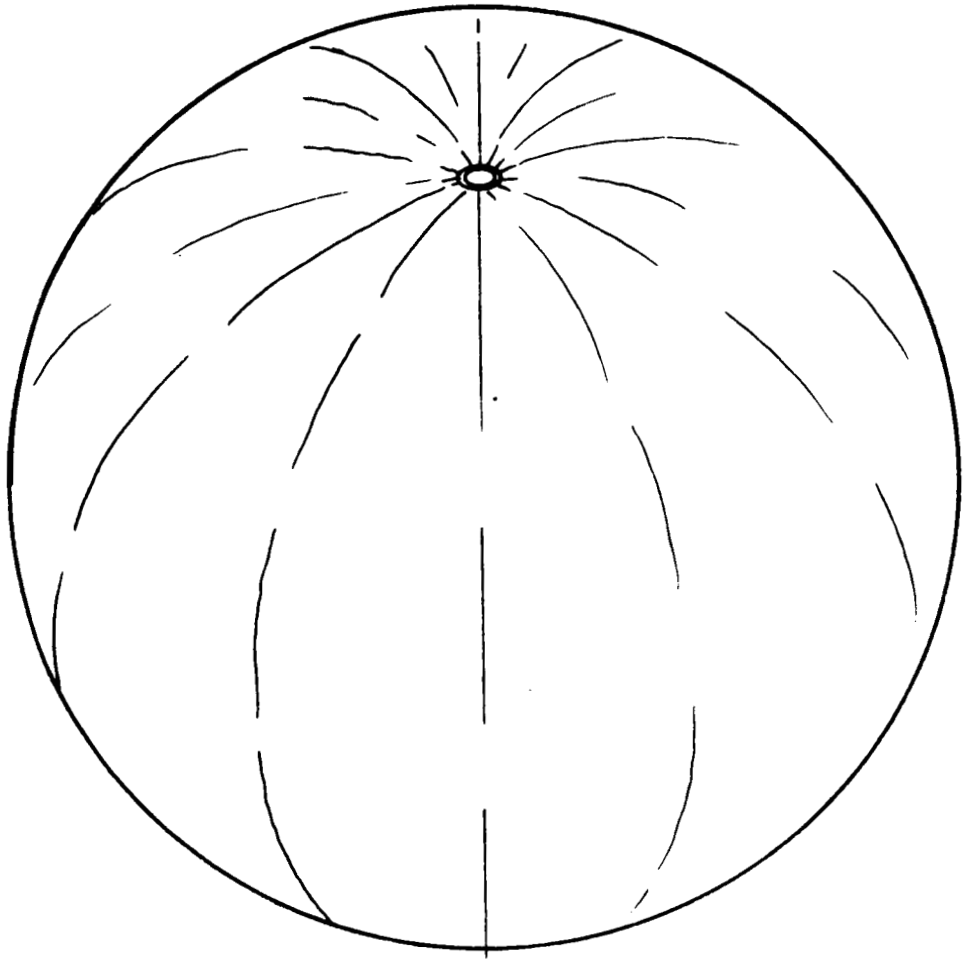

Figure 3.- Schematic of 30.48-m diameter PAGEOS sphere (Tilted forward to show end cap).

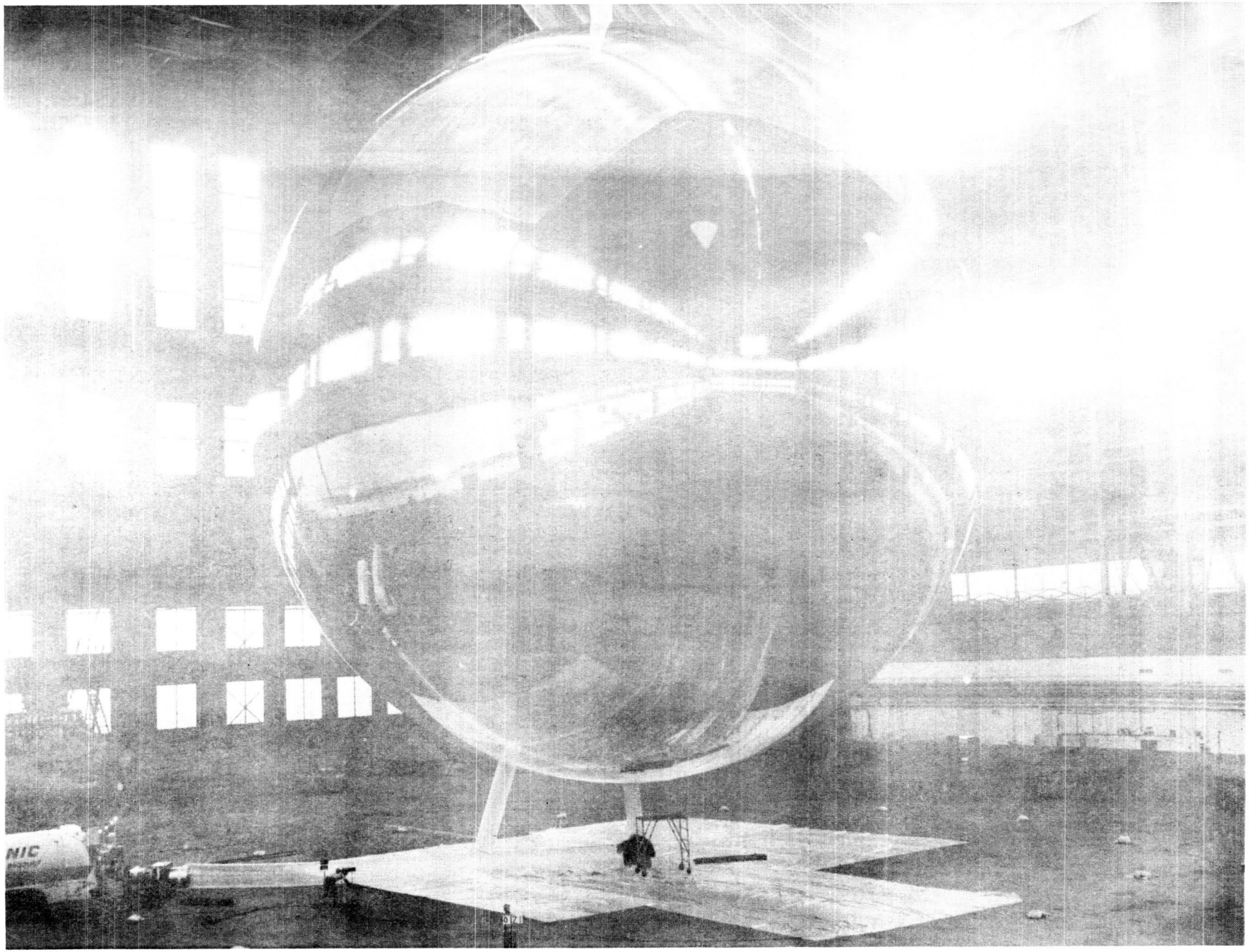

Figure 4. — PAGEOS sphere during static inflation test

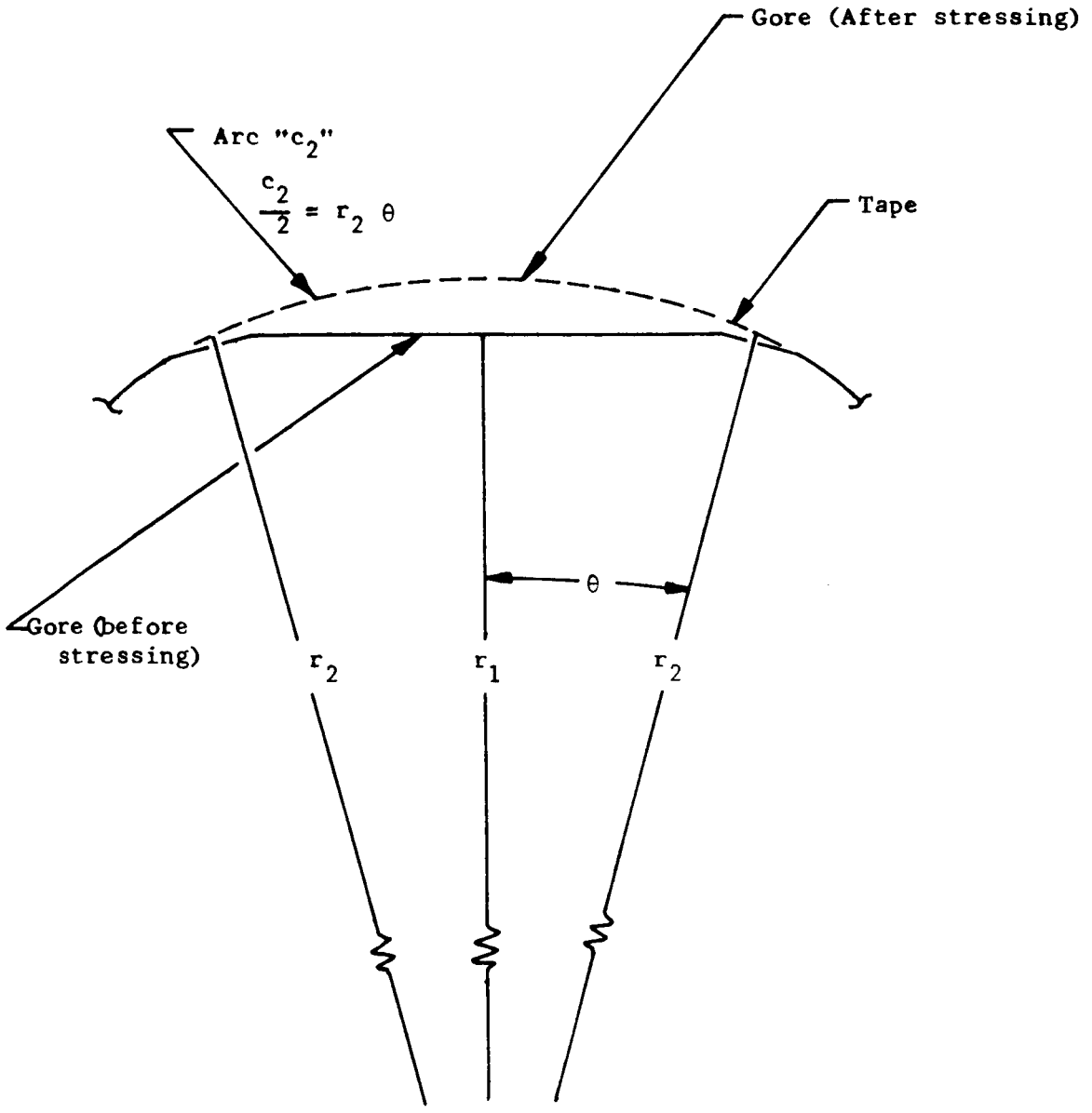

Figure 5.- Stretching material to produce sphere from flat panels.

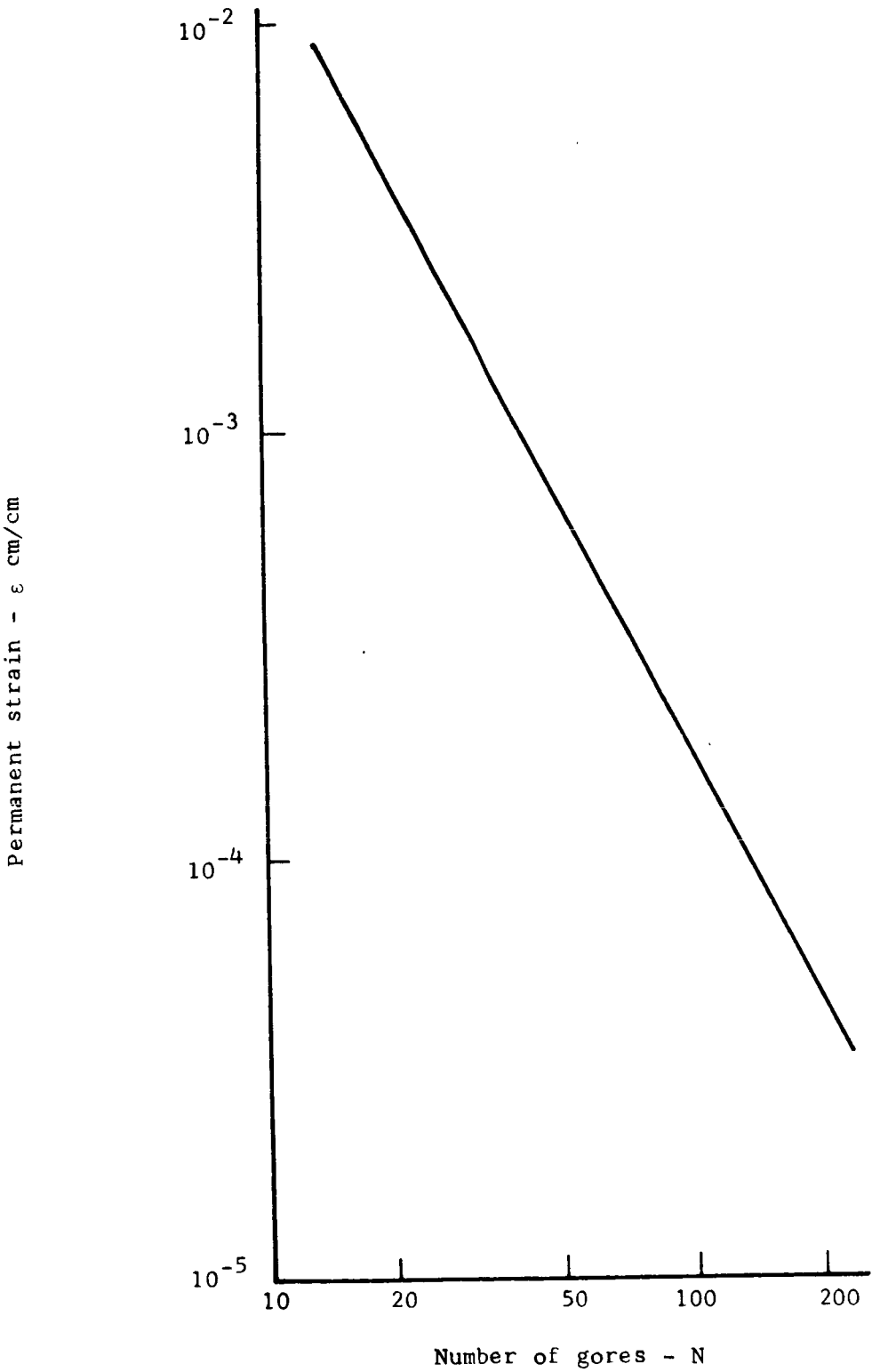

Figure 6.- Permanent strain required to remove gore flats vs number of gores.

The corresponding intersection with the curve fixes the required stress. Figure 7 shows that a material stress of approximately 545 x 10^6 dyn/cm^2 will yield the desired permanent deformation.

The pressure required to attain the desired permanent elongation may be calculated from the equation S = p r/2t,

as $p = 0.0908 \times 10^4$ dyn/cm^2

since $t = .0127$ mm

$S = 545 \times 10^6$ dyn/cm^2

and $r = 15.24$ meters

Figure 8 shows the stress plotted as a function of pressure.

Tapes.—The gore tapes represent an irregularity on the sphere surface. At the joint, two thicknesses of material are present, and two stress conditions exist in the composite made up of gore, tape, and adhesive. One biaxial stress condition occurs in the composite, and the second occurs in the tape itself in an area defined by the gap between adjacent gores and the tape length. The conditions are illustrated in figures 9 and 10.

Abrupt thickness transitions such as those at the taped junctions might be expected to cause stress concentrations, on the order of two to three times the stress at a distance from the tape. However, extensive testing, and experience with PET and PET inflatables, has demonstrated that stress concentrations do not occur or are insignificant if present.

Assuming that the stress conditions illustrated in figure 10 are realized, and that inflation pressures are great enough to achieve the desired permanent gore deformation, the principal effect of the tapes will be a longitudinal restraint. Tape elongation will be within the elastic range of PET so that with subsequent release of internal pressure, the tapes will return to their unstressed position.

It follows from the above discussion, that it is reasonable to expect that loading of the polar caps will be circumferentially uniform. Therefore, edge loading strain will be divided equally between the two polar caps at each polar location resulting in a uniform biaxial stress in each. Equations for stress are as follows:

Edge loading at periphery of caps

$Q = S_{skin}\, t_{skin}$,

$t_{skin} = 0.0127$ mm

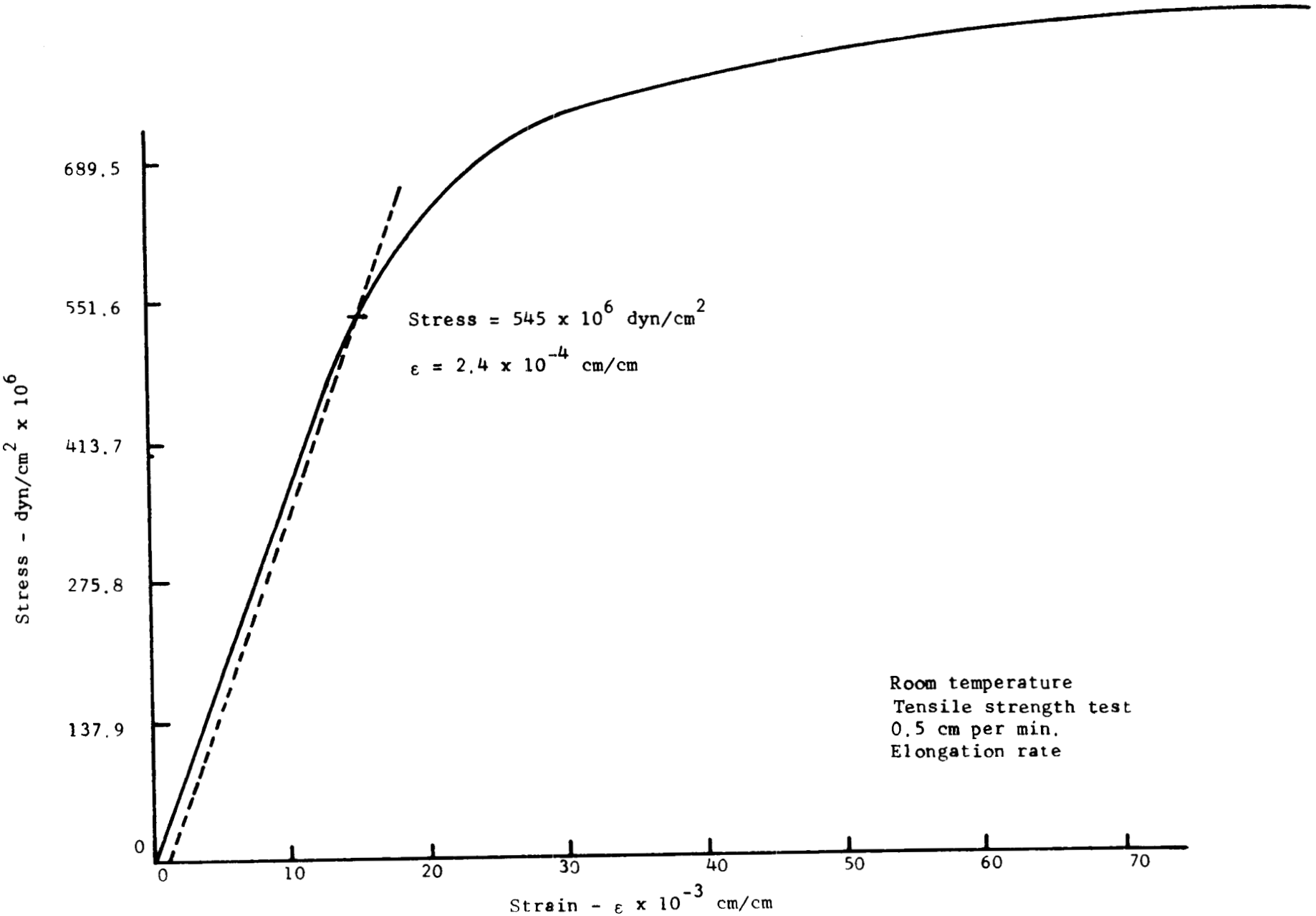

Figure 7.- Stress vs strain PET

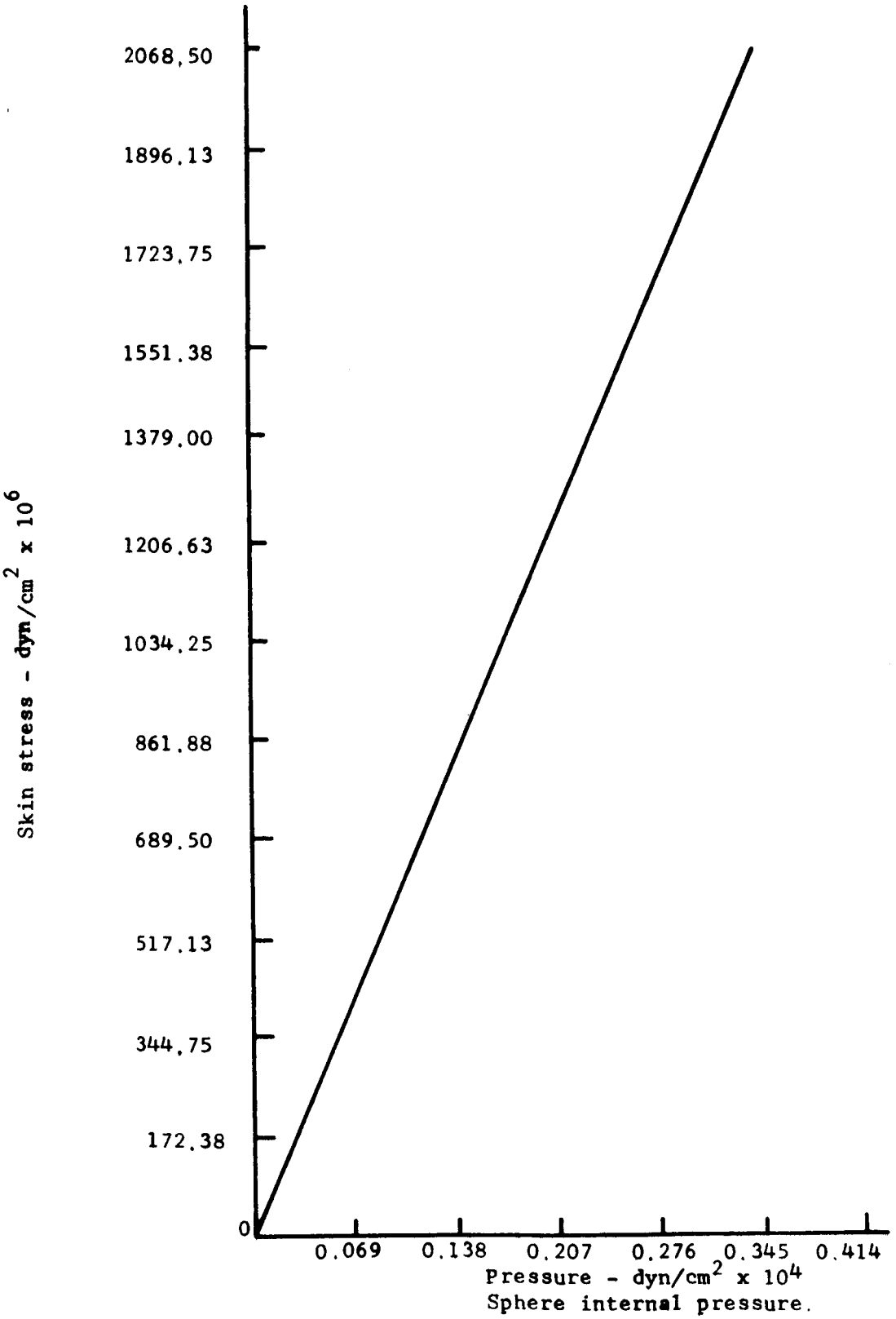

Figure 8.- Skin stress vs internal pressure 30.48-m diameter PAGEOS sphere.

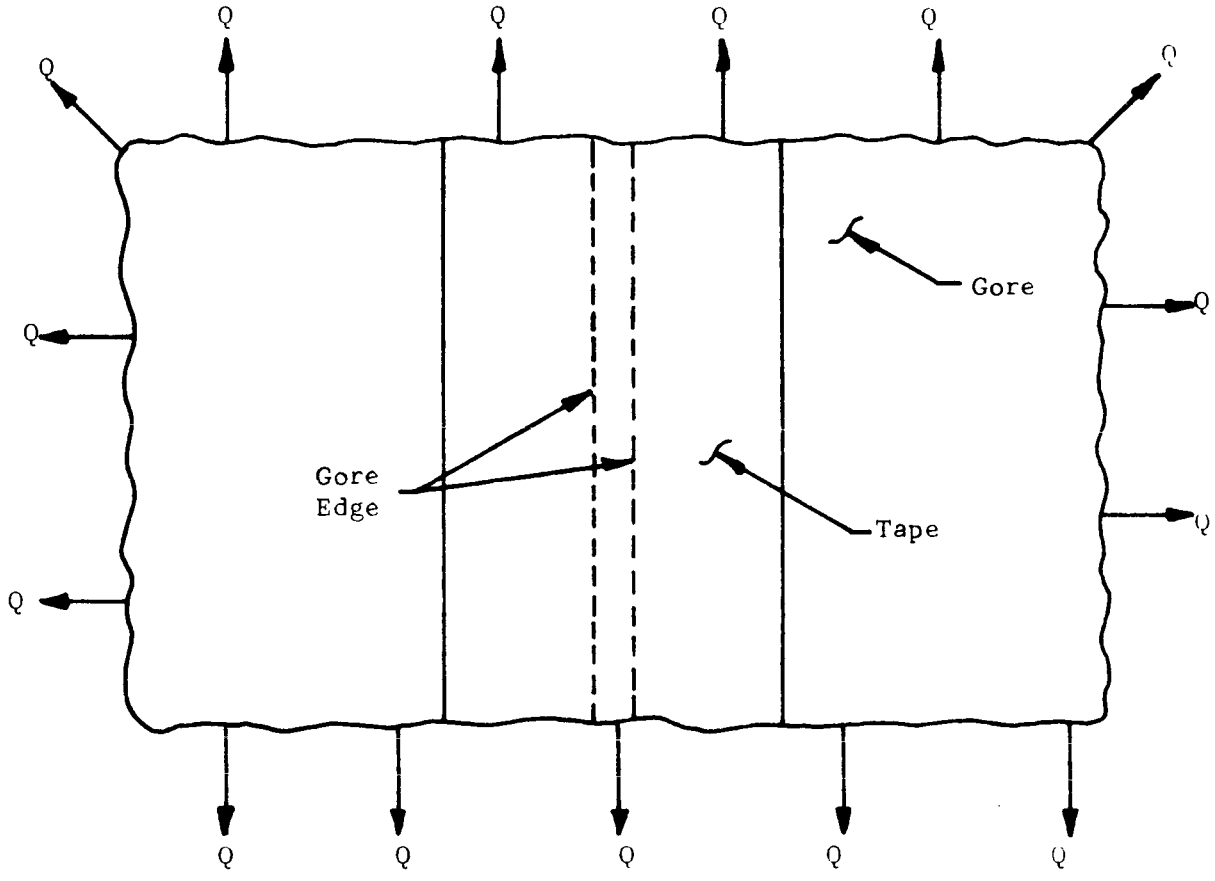

$Q = S_{Skin}\ t_{Skin}$

Q is assumed to be uniform loading caused by uniform internal pressure

Figure 9.- Loading of tape-gore composite.

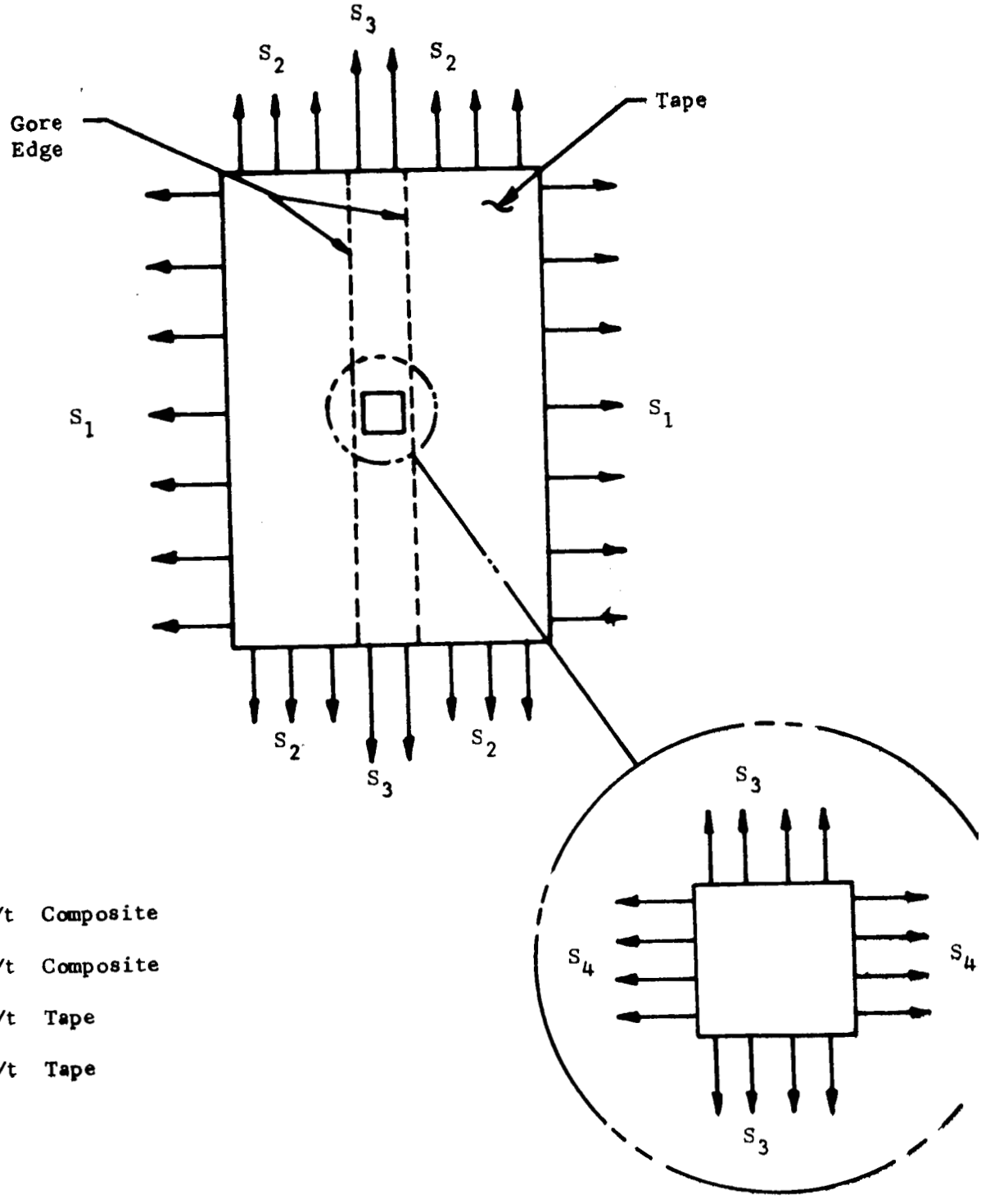

$S_1 = Q/t$ Composite

$S_2 = Q/t$ Composite

$S_3 = Q/t$ Tape

$S_4 = Q/t$ Tape

Figure 10.- Stress distribution tape-gore composite.

Inner polar cap stress

$$S_i = (Q) \Big/ t_{\text{polar cap}},$$

$$t_{\text{polar cap}} = 0.0254 \text{ mm} = 2t_{\text{skin}} ;$$

$$\therefore S_i = \frac{Q}{2t_{\text{skin}}} = \frac{S_{\text{skin}}}{2}$$

This indicates that the inner polar cap is twice as strong as the rest of the sphere, and hence has a safety factor of two. Moreover, the outer polar cap, serving as a uv shield, adds additional strength.

Stress Analysis Static Inflation Test Sphere

The static inflation test sphere is similar to the flight sphere with the exception of inflation ducts, valve duct, and equatorial load patches. Therefore, the preceding discussion applies to the test sphere as well as the flight sphere with the exception of items mentioned.

Inflation ducts.—Since the duct cut-out is overlaid with a fabric disc, it is assumed that no discontinuities are present in the sphere skin, and the comments above regarding polar caps are directly applicable. A safety factor has been included in the design because of dynamic loading during inflation. The safety factor may be determined as follows:

Accepted ultimate strength of 0.0127-mm PET = 1.75×10^6 dyn/cm

Measured ultimate strength of fabric

(a) Woof = 5.26×10^6 dyn/cm

(b) Warp = 5.61×10^6 dyn/cm; therefore,

Safety factor ≈ 3

Valve duct.—Loading conditions for the various elements of the valve duct assembly are shown in figure 11. Each element can be analyzed as follows:

1. Fabric tape ring:

$$Q/2 = 1/2 \left[\text{Stress}_{\text{skin}}\right] \left[\text{thickness}_{\text{skin}}\right] ,$$

A. Reinforcement of cut-out with fabric and line

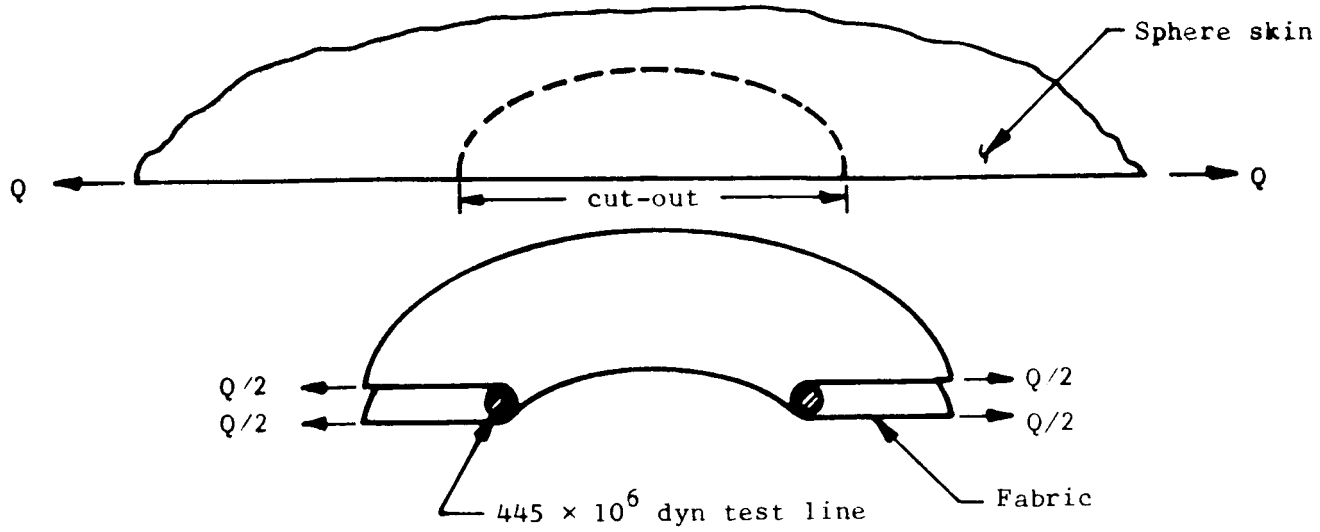

B. Reinforced valve duct assembly

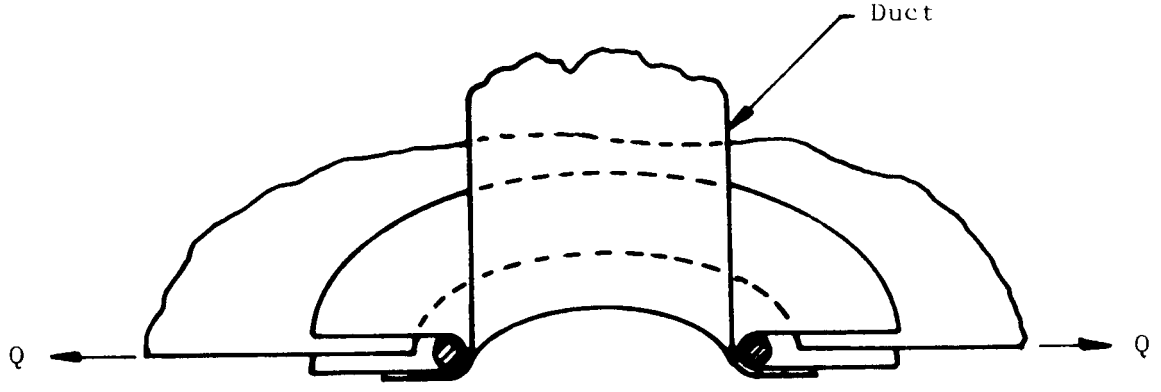

(Q is effective uniformly around the perimeter)

Figure 11.- Valve duct loading

Ultimate strength of fabric = 5.26×10^6 dyn/cm

Ultimate design load of sphere skin = Q = 1.75×10^6 dyn/cm

Fabric loading = Q/2 = 0.87×10^6 dyn/cm

Safety factor ≈ 6

2. 445×10^6 dyn line

Loading = P = $\frac{Q\ell}{2}$,

ℓ = (πD) = 2.39 meters

P = 209.6×10^6 dyn

Safety factor ≈ 2

3. Valve duct

Hoop stress = Q = 1.75×10^6 dyn/cm

Ultimate strength of laminate = 5.26×10^6 dyn/cm

Safety factor ≈ 3.

As for polar cap loading, the assumption has been made that the adhesive used provides a uniform loading free of stress concentrations.

Equatorial load patches.—The load patch analysis is as follows:

1. Sphere material

Ultimate strength = 1.75×10^6 dyn/cm

Bond length for patch = 96.5 cm

Maximum allowable patch loading = 169.1×10^6 dyn

2. Load patch material

Ultimate strength of nylon 4.71×10^6 dyn/cm

Maximum allowable material loading = $(4.71 \times 10^6)(96.5) = 454.3 \times 10^6$dyn

Safety factor ≈ 2.7

3. Load attachment belting (see figure 12)

Ultimate load cotton belt = 44.5×10^6 dyn

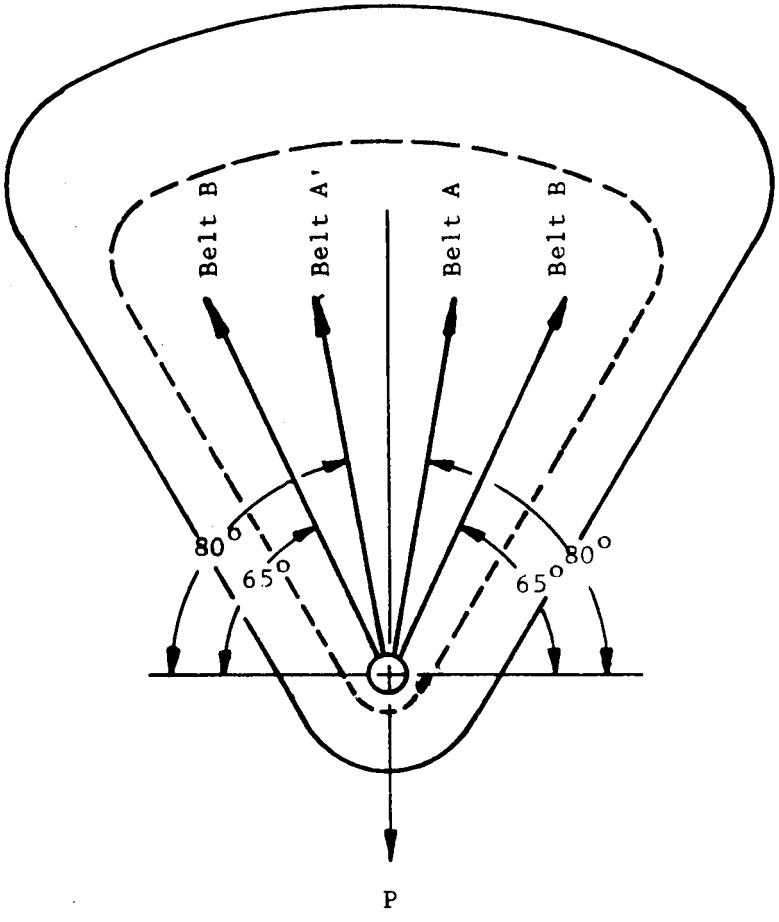

Maximum allowable load - P dynes

Maximum allowable load belt A = Belt B = Belt A' =

Belt B' = 44.5×10^6 dyn

Allowable Load

$P = 2(44.5 \text{ SIN } 80^\circ) + 2(44.5 \text{ SIN } 65^\circ) = 168 \times 10^6$ dyn

Figure 12.- Load attachment belting for SIT load patches.

From this, it can be seen that the load attachment belting is well matched to the maximum stress developed in the PET during pressurization. However, the anticipated maximum loading for each load patch is 22.6×10^6 dyn/cm. Therefore, the design provides a safety factor of about 7.

Thermal Analysis

In NASA TND-115 it is shown that the rate at which the sphere absorbs direct sunlight is:

$$\frac{\pi D^2}{4} C_S A_S$$

The rate at which the sphere absorbs solar radiation which has first been reflected from the earth is:

$$\frac{\pi D^2}{4} C_S A_S \, a \, f_1(k)$$

where:

$$f_1(k) = \frac{4}{3k} \left[1 + \frac{k^3}{3} - \left(1 + \frac{k^2}{2}\right) (1 - k^2)^{1/2} \right]$$

and

$$k = \frac{r_E}{r_E + h}$$

The rate at which the sphere absorbs infrared radiation emitted by the earth is:

$$\frac{\pi D^2}{4} C_S A_E \, \frac{1 - a}{2} f_2(k)$$

where:

$$f_2(k) = \left[1 - (1 - k^2)^{1/2} \right]$$

Summing these three sources of energy to the sphere and equating the sum to the rate ($\pi D^2 e_o \sigma \overline{T^4}$) the sphere emits energy, yields:

$$\pi D^2 e_o \sigma \overline{T^4} = \frac{\pi D^2}{4} C_S A_S \left[1 + a \, f_1(k) + \frac{A_E}{A_S} \, \frac{1 - a}{2} f_2(k) \right]$$

Solving for the mean temperature yields:

$$(\overline{T^4})^{1/4} = \left(\frac{C_S}{\sigma}\right)^{1/4} \left(\frac{A_S}{4e_o}\right)^{1/4} \left[1 + a\, f_1(k) + \frac{A_E}{A_S}\,\frac{1-a}{2}\, f_2(k)\right]^{1/4} \qquad (3)$$

Therefore if direct sunlight contributes 100 units of energy per second to the sphere (first term of the third multiplier above) then earth albedo (second term) contributes about ten, and earth infrared (third term) about two.

Evaluating equation (3) using the values below,

$$C_S = 2.00 \text{ cal/cm}^2 \text{ minute}$$

$$\sigma = 5.672 \times 10^{-5} \text{ ergs/cm}^2\text{sec}^{\circ}\text{K}^4$$

$$A_S = 0.1$$

$$e_o = 0.03$$

$$A_E = e_o$$

$$k = r_E/(r_E + h)$$

yields Table 1 for the mean temperature.

TABLE 1

h Km \ a	0.36	0.52	0.85
4500	115.6 C	118.9 C	125.4 C
4247	116.2 C	119.6 C	126.6 C
4000	116.8 C	120.5 C	127.8 C

It is concluded that the sphere's mean temperature is around 120 C and deviates from 120 C by less than $\pm$ 10 C due to expected variations in h and a.

It is of interest to examine the sensitivity of the sphere's mean temperature to uncertainties in aluminizing emittance e. Three values of e_o are considered; 0.03, 0.04, 0.05, and the results appear below.

e_o	$(\overline{T^4})^{1/4}$ (°C)
0.03	116.2
0.04	89.7
0.05	70.5

It is concluded that $(\overline{T^4})^{1/4}$ is quite sensitive to variation of e_o. In this report the lower limit on e_o for aluminized PET is taken as 0.03.

The temperature on the sphere at the point nearest the sun is given by

$$T_{HS} = \left[\frac{C_S}{\sigma}\right]^{1/4} \left[\frac{A_S}{e_i + e_o}\right]^{1/4} \left[1 + \frac{e_i}{4e_o}\left(1 + af_1(k) + \frac{A_E}{A_S}\,\frac{1-a}{2}\,f_2(k)\right)\right]^{1/4} \quad (4)$$

The emittance of the PET side of PAGEOS material was measured with an emissometer. The reading obtained was $e_i = 0.49$. Putting this result in the expression for T_{HS}, and the previously used values of C_S, A_S, e_o, and A_E in conjunction with the standard orbit yields $T_{HS} = 129.8$ C, 13.6 C over the 116.2 C mean temperature.

The temperature of a gore seal in the vicinity of a hot spot, assuming that the thermal conductivity of aluminized PET is negligible, is

$$T_s = \left[\frac{C_S}{\sigma}\right]^{1/4} \left[\frac{A_S}{2e_A}\right]^{1/4} \left[1 + \left(\frac{1}{4}\;1 + a\,f_1(k) + \frac{A_E}{A_S}\;\frac{1-a}{2}\,f_2(k)\right)\right]^{1/4} \quad (5)$$

The result for T_s is 205.4 C. If the previous calculations were repeated using $A_s = 0.12$ rather than 0.10, T_s would have been 227.7 C.

It is concluded that if the thermal conductivity of aluminized PET were zero, a seal on the sphere's hot spot would come to an equilibrium temperature near 200 C.

The theoretical model of a seal analyzed here deviates in some respects from the true situation. (1) The gore material is assumed to extend infinitely to the right and to the left of the seal considered. Nevertheless, the equilibrium temperature of this material at any distance X, in the absence of a seal at X = 0, is assumed to be the hot spot temperature T_{HS}. (2) The 0.0127 mm aluminized PET used in both gore and seal is taken as having an aluminum deposit 2300 Å thick. The thermal conductivity of this aluminizing is assumed to be the same as that of bulk aluminum. (3) The presence of 0.0127-mm adhesive between the seal and the gore is neglected. The thin aluminizing distributes heat about 25 times better than 0.0127-mm PET. Consequently, neglecting the adhesive introduces an error into the effective thermal conductivity of the seal of less than 2 per cent. (4) It is assumed that there

is no temperature variation within the material in the thickness direction. This is not true at the seal edges where the aluminizing on the seal ends abruptly.

The theoretical model gives the temperature at the center of the seal as lying somewhere between 183.3 C and 184.9 C.

It is concluded that the thermal conductance of the aluminized PET can lower the temperature at the center of a seal on the hot spot by as much as 20 degrees Celsius, compared to the case where the effect of thermal conductance is assumed to be absent.

Inflation System

The inflatant system of a PAGEOS sphere consists of a mixture of two powdered organic compounds, anthraquinone and benzoic acid. The weight of the two inflatant powders taken together was set at 13.6 Kg. After inflation, but prior to vapor loss through vent holes, the skin stress desired in a PAGEOS sphere is 48.3×10^6 dyn/cm^2. The gas pressure inside the sphere requir to give this skin stress will now be found.

The relationship between internal gas pressure and skin stress is $p = 2\,St/r$. For the PAGEOS sphere

$$S = 48.3 \times 10^6 \text{ dyn/cm}^2$$

$$t = 0.0127 \text{ mm}$$

$$r = 15.2 \text{ m}$$

Consequently, the required gas pressure p is 80.71 dyne/cm^2.

An expression for the vapor pressure p_v of anthraquinone as a function of temperature is given in NASA-TND-2194 as

$$\ell n\, p_v = 40.145 - \frac{15206}{T}$$

Here p_v is the vapor pressure expressed in dyn/cm^2 while T is the temperature in degrees K. The cold spot temperature, T_{cs}, on a PAGEOS sphere will be substituted for T for the reasons dealt with below.

After sphere inflation (any effect of vent holes in the sphere is not considered here) not all of the anthraquinone is vaporized; anthraquinone vapor will exist in equilibrium with the solid. It is expected that solid anthraquinone near the sphere hotspot will sublime, move across the sphere, and condense on the cooler surface of the sphere. In what follows it is assumed that the sphere is in polar orbit and that the coldest spot on the sphere does not change position in time, i.e., that PET which is the coldest at sometime is the coldest for all time. Eventually, it is expected that all solid anthraquinone will end up near the coldest spot of the sphere.

The pressure of anthraquinone gas in the PAGEOS sphere is expected to be the same as the vapor pressure of anthraquinone at the coldspot temperature of the sphere. There is the question as to what this coldspot temperature is. A seal on the cold side of the sphere cannot be cooler than an adjacent gore since, if it was cooler, anthraquinone would condense on the seal. This would change the emittance of the aluminized seal from 0.03 to that of anthraquinone. The emittance of anthraquinone, measured with an emissometer, is above 0.47 which is comparable with the emittance of the PET forming inside of a gore. Consequently the seal would be expected to become indistinguishable in thermal properties from the surrounding gore and therefore come to the same temperature as the surrounding gore.

The expression for the coldspot temperature T_{cs} of a PAGEOS sphere in its launch orbit is obtained by neglecting terms associated with direct and indirect sunlight, i.e. earth albedo.

The result is:

$$T_{cs} = \left[\frac{e_i}{e_i + e_o}\right]^{1/4} \frac{}{T^4}^{1/4} + \left[\frac{C_S}{\sigma}\right]^{1/4} \left[\frac{A_S}{e_i + e_o}\right]^{1/4} \left[\sqrt{5k}\left(\frac{1-a}{4}\right)\frac{A_E}{A_S}\frac{0.0843}{\pi}\right]^{1/4} \quad (6)$$

The various quantities in the expression above are given the values shown below.

$$e_i = 0.49$$

$$e_o = 0.03$$

$$\frac{}{T^4}^{1/4} = 381.7\text{K}$$

$$C_S/\sigma = (396.0\ \text{K})^4$$

$$k = 0.6$$

$$a = 0.36$$

$$A_E = e_o = 0.03$$

$$A_S = 0.12$$

The result for T_{cs} is 376.1 K or 102.9 C.

When the previous value for T_{cs} is substituted into the expression for the vapor pressure p_v of anthraquinone, one obtains $p_v = 0.75$ dyn/cm^2. The anthraquinone gas pressure inside a PAGEOS sphere will equal $p_v = 0.75$ dyn/cm^2 provided that enough solid anthraquinone is initally put into the sphere. The minimum amount required was computed assuming that the vapor obeys

the perfect gas law, an assumption which is nearly true at the low pressures dealt with here, and the T_{cs} derived above. Consequently, 0.356 moles are required. Since the molecular weight of anthraquinone is 208.2, 0.356 moles corresponds to 74 grams. Much more than 74 grams of solid anthraquinone was to be inserted into a PAGEOS sphere. Consequently, the portion of the total gas pressure in the sphere caused by the anthraquinone was 0.75 dyn/cm^2. The portion of the total gas pressure caused by benzoic acid will be computed next.

The total gas pressure inside a PAGEOS sphere is to be 80.71 dyn/cm^2. Since anthraquinone contributes 0.75 dyn/cm^2, the benzoic acid must contribute 79.79 dyn/cm^2. The question of whether benzoic acid has a vapor pressure greater than or equal to 70.79 dyn/cm^2 will be investigated first. An expression for the vapor pressure of benzoic acid as a function of temperature is given in NASA-TND-2194 as

$$\ell n\, p_v = 29.595 - \frac{8223}{T} . \qquad (7)$$

Here p_v is the vapor pressure of benzoic acid expressed in dyn/cm^2, and T is the temperature in degrees K. Substituting the coldspot temperature (T_{cs} = 376.1 K) into this expression results in a p_v = 2275 dyn/cm^2.

All of the benzoic acid put into a PAGEOS sphere sublimes into the vapor phase soon after sphere inflation, at which time the benzoic acid gas pressure is to be 79.79 dyn/cm^2. Assuming that the benzoic acid vapor obeys the perfect gas law, which is nearly true at these low pressures, and since the benzoic acid vapor is in contact with all portions of the sphere, it seems natural to take the mean temperature of the sphere (108.5 C) as the temperature of the benzoic acid vapor rather than the coldspot temperature (102.9 C). Computing 36.8 moles are required. Since the molecular weight of benzoic acid is 122.12, the benzoic acid weight required is 4.50 Kg.

Since 4.5 Kg of benzoic acid are required, and since the total inflatant weight is fixed at 13.6 Kg, 9.1 Kg of anthraquinone should be put into a PAGEOS sphere.

The graph which follows (figure 13) indicates how much the skin stress can deviate from 48.3 x 10^6 dyn/cm^2 due to either an error in the number of kilograms of benzoic acid placed inside the sphere or to an error in the temperature of the benzoic acid vapor. No error in the coldspot temperature is allowed for in this graph. Consequently, the portion of the skin stress caused by the anthraquinone vapor (45.5 x 10^4 dyn/cm^2) is constant in the graph which follows.

Chemical Treatment

During the fabrication of the static inflation test prototype sphere, it was discovered that the aluminized PET would adhere to itself and form a bond stronger than the material. Attempts to separate the material caused it to tear. Six torn areas were discovered during inspection of this sphere prior to shipment, and three additional discovered during erection. One

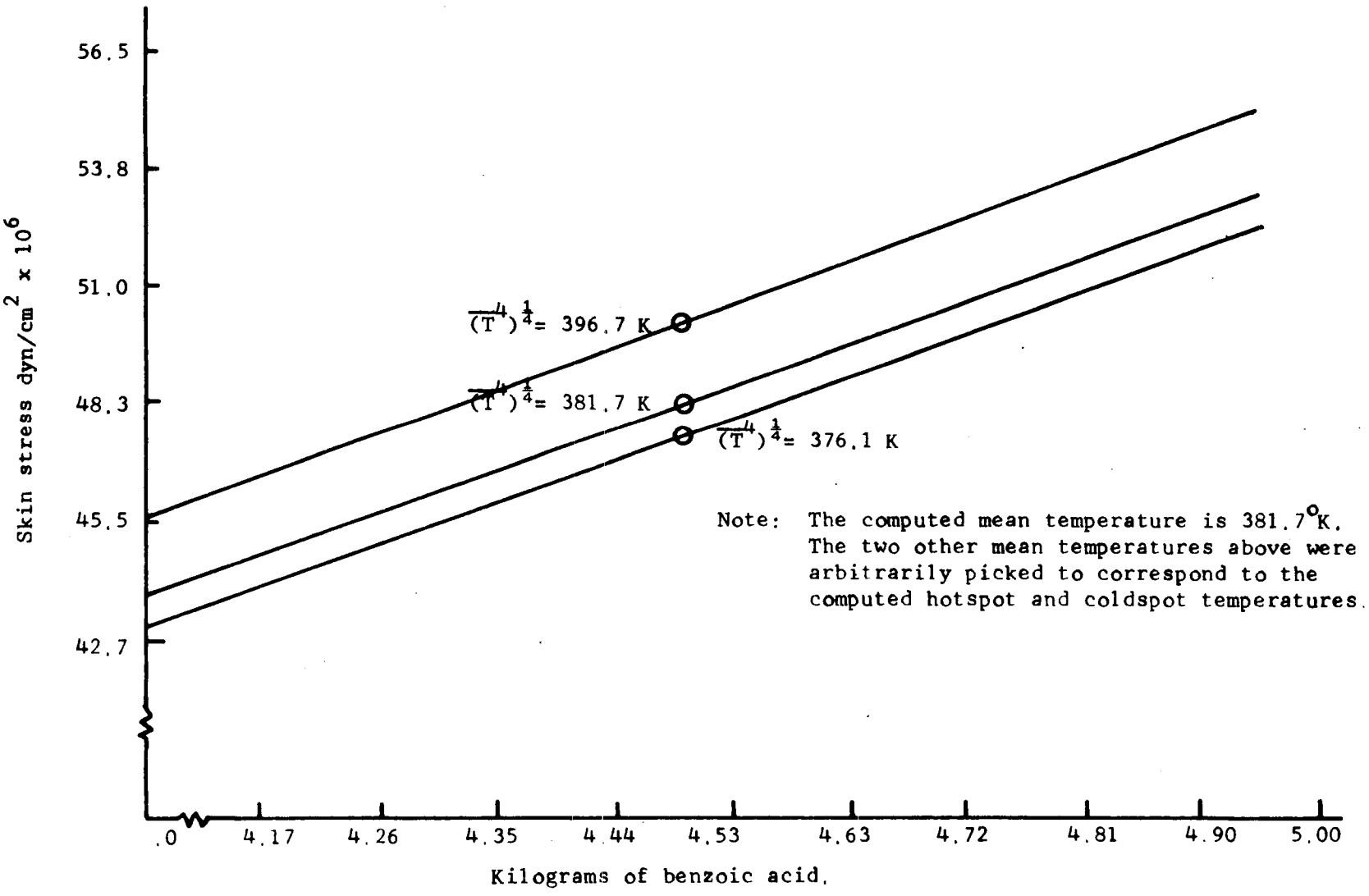

Figure 13.- Skin stress versus kilograms of benzoic acid vapor inside the sphere for three temperatures.

area remained undetected until it was discovered during the failure analysis of the ruptured sphere.

Adhered areas of the type discovered could cause a catastrophic rupture of a deploying inflatable sphere in a space environment. Therefore, it was necessary to take corrective action to preclude blocking in the flight article spheres. It was decided that the PET be chemically treated with a solution of Freon[1] and a cationic detergent to eliminate surface adhesion. This appeared to be promising in small-scale laboratory tests, and accordingly a study of this technique, and design and construction of a machine which could treat the PET was undertaken.

Material was treated with 53 parts per million (ppm), active ingredients of the cationic detergent in Freon-TF. A treatment threshold level[2] of 35 ppm was found and multiplied by 1.5, representing a 50 per cent safety factor added to this threshold level. The resulting value of 52.5 was rounded to 53. This is equivalent to 200.6 milliliters of the cationic detergent in every 3.785 litres of Freon-TF.

It was found by statistical analysis that treating by a 24-hour soaking method does not significantly degrade the tensile strength of the material in the machine direction, but it significantly degrades the seam creep properties. The average degradation is 0.033 mm with a 90 per cent confidence level that it does not exceed 0.061 mm.

The reverse roll method ultimately used in the design of the machine does not significantly degrade the material tensile strength before and after thermal shock, flexure, or impact. Neither did it affect the aluminum adhesion, reflectance, specularity, resistivity, or the results of thermal vacuum, seam creep, or seam peel tests.

Table No. 2 entitled "Summary of Quantitative Analyses" summarizes the statistical conclusions.

DESIGN TESTING

Static Inflation Test

The PAGEOS static inflation test was conducted at the Naval Air Station, Lakehurst, New Jersey, in a large dirigible hangar to prove the quality of design, material, and fabrication methods used in the end-item orbital sphere. In such a test many difficulties are encountered in attempting to duplicate the environment in which the satellite must function, as the end item sphere

---

[1] du Pont TM Registered

[2] Threshold level means the minimum treatment bath concentration level required to eliminate blocking.

TABLE 2.- SUMMARY OF QUANTITATIVE ANALYSES

Test Title	Test Code	X & Y Identification	(1) $\bar{X} - \bar{Y}$	(2) $U_{\mu_x - \mu_y}$	(3) Conclusion from Test of Hypothesis
SOAK TESTS	---	--------	-------	-------	
Tensile Strength (M.D.) ($dyn/cm^2 \times 10^6$)	---	X = Untreated Y = Treated	4.1	83	$\mu_x \leq \mu_y$
Seam Creep (mm)	---	X = Treated Y = Untreated	0.033	0.061	$\mu_x \geq \mu_y$
REVERSE ROLL TESTS	---	--------	--------	--------	
Tensile Strength (M.D. & T.D.) ($dyn/cm^2 \times 10^6$)	1	X = Untreated Y = Treated	-12.4	37.2	$\mu_x \leq \mu_y$
Machine Direction ($dyn/cm^2 \times 10^6$)	1A	X = Untreated Y = Treated	12.4	56	$\mu_x \leq \mu_y$
Transverse Direction ($dyn/cm^2 \times 10^6$)	1B	X = Untreated Y = Treated	-36	15	$\mu_x \leq \mu_y$
Tensile Impact (M.D. & T.D.) (dynes $\times 10^6$)	2	X = Untreated Y = Treated	0.33	0.60	$\mu_x > \mu_y$
Machine Direction (dynes $\times 10^6$)	2A	X = Untreated Y = Treated	0.78	1.22	$\mu_x > \mu_y$
Transverse Direction (dynes $\times 10^6$)	2B	X = Untreated Y = Treated	-0.13	0.16	$\mu_x \leq \mu_y$
Thermal Shock ($dyn/cm^2 \times 10^6$)	3	X = Untreated Y = Treated	-14	52	$\mu_x \leq \mu_y$

TABLE 2.- SUMMARY OF QUANTITATIVE ANALYSES (concluded)

Test Title	Test Code	X & Y Identification	$\bar{X} - \bar{Y}$	$U_{\mu_x - \mu_y}$	Conclusion from Test of Hypothesis
Seam Creep (mm)	4	X = Treated Y = Untreated	0.010	0.038	$\mu_x \leq \mu_y$
Flexure ($dyn/cm^2 \times 10^6$)	6	X = Untreated Y = Treated	-12	25	$\mu_x \leq \mu_y$
Reflectance and Specularity	9	--------	--------	--------	
Reflectance	9A	X = Untreated	-0.076%	0.010%	$\mu_x \leq \mu_y$
Diffusion	9B	X = Treated Y	0.103%	0.220%	$\mu_x \leq \mu_y$
Resistivity (ohms/sq)	10	X = Treated Y = Untreated	-0.138	-0.1120	$\mu_x \leq \mu_y$
Thermal Vacuum	12	--------	--------	--------	
$22^o \pm 1^o$ C	12A	X = Treated Y = Untreated	--------	--------	
$65^o \pm 1^o$ C	12B	X = Treated Y = Untreated	-0.075 mg	-0.041 mg	$\mu_x \leq \mu_y$

(1) $\bar{X} - \bar{Y}$ - Difference between sample mean of X and sample mean of Y

(2) $U_{\mu_x - \mu_y}$ - Upper 90% confidence limit for the degrading difference between population means of X and Y

(3) $\mu_x > \mu_y$ - Population mean of X is significantly greater than population mean of Y at the 90% level of confidence

will be free of any attachments, fittings, control and measuring devices, and will be in a zero-gravity, space environment.

To conduct the static inflation test, several modifications had to be incorporated into the test sphere to facilitate positioning and instrumentation during the test. Such modifications included attachments by which the sphere can be anchored to minimize motion (tie-down patches), pressure taps, an inflation port, and exhaust ports. There were three ports on the test sphere: one on top, one on the bottom and one in the inlet inlet and in the form patches evenly spaced around a line 3.048 m above the equator.

Tie-down patches. The specific objective of this test was to check the reliability and strength of the tie-down system to be used on the PAGEOS static inflation test sphere.

The configuration of the tie-down patch tests is shown in the accompanying photograph (Figure 14). A test fixture was suspended from an overhead beam. This fixture was composed of two wooden frames and a means of clamping them tightly together.

The test specimen was a load patch bonded to the metallized surface of PET. A seam in the material was made on either side of the patch. This provided an approximate duplication of the actual position of the patch on a gore of the static inflation test sphere.

A weight holder was fastened to the load patch. Above the patch three extensometers were fastened to the PET when the system was in a relaxed state, so that the gages had an initial reading of zero.

The large piece of PET was clamped smoothly, without stretching, around the perimeter of the wooden test fixture. Three black ink lines were placed on the upper arc of the patch, each line centered on the outer edge of the bond area. This was done so that any creep of the loaded patch from its unloaded position would be clearly indicated by a fine silver line appearing in the blackened area.

The weight increments used in applying the load weighed 4.536 Kg. The load container and its attachment also weighed 4.536 Kg.

The first four loading cycles were conducted with the load patch at 10 degrees from the vertical. The tie-down patch was loaded incrementally to destruction. The test was conducted at a relative humidity of 49 per cent, and a temperature of 22 C.

Minor separation of metalizing to PET around inside edge of bond area and about 15.2 to 25.4 cm above bottom of patch occurred at 109 Kg load. and skin fractures were observed at 159 Kg in the area where the metalizing first began separating from the PET. These were first noticed as small slits about 1.27 cm long, but propagated very slowly inward and downward from both sides of the patch bond as the loading was increased. This was the only location of skin failure prior to complete failure of the patch. The O-ring of the patch broke at 81.7 Kg load because of a flaw in the ring. The test was

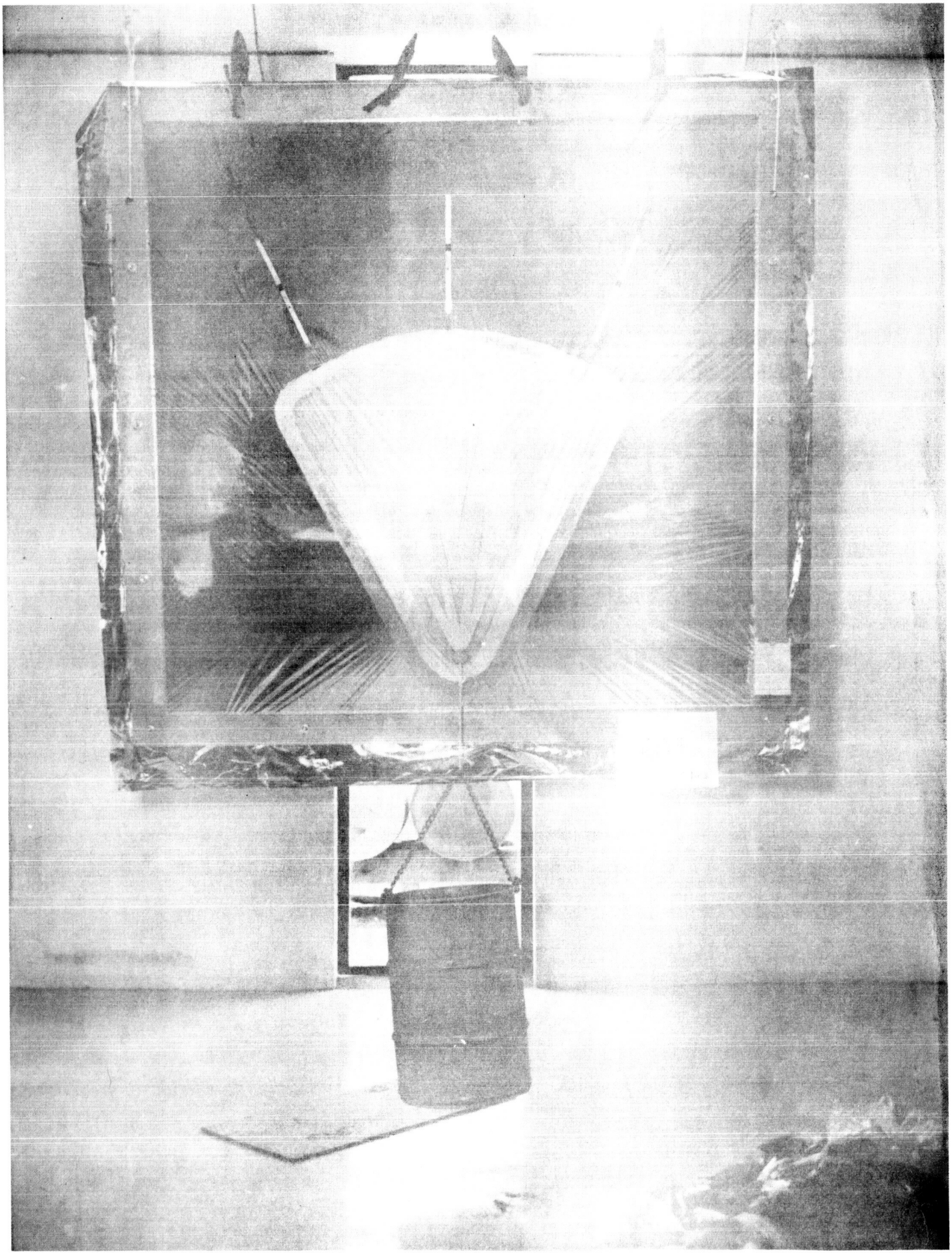

Figure 14. — Tie down patch under test

continued by looping the cord through the cotton belting. This began to fray at the point where the cord was tied at the bottom when the loading was 172 Kg. The tie-down patch failed when loaded to 195 Kg. Failure was a crosswise rip through the center of the patch just above the upper ends of the cotton belting. No signs of adhesive creep or failure were noticed at any time. The metalized PET directly above the patch did not develop cracks.

It was shown that:

1. The load capacity of the tie-down patch far exceeded the test requirements and its attachment was reliable. Because of this, no local stress concentrations were expected on the static inflation sphere.

2. The adhesive used formed an excellent bond to the metallized surface and exhibited no indication of creep.

3. The nylon patch distributed the load properly.

Spherical segment.—The objective of the spherical segment tests was to compare the ultimate bursting strength of modified segments of a PAGEOS sphere to an unmodified polar cap segment, to ascertain the design worthiness of each duct configuration and demonstrate reliability of design. Another test objective was to check fabrication procedures and methods to insure against irregularities occurring in the modified areas of the sphere.

The 4.57-m diameter test segment was clamped tightly to the floor by a steel ring about its circumference. The ring was fitted with a rubber gasket and bolted onto the floor. A ring of tape with adhesive on both sides was put down on the floor under the ring. The test segment was clamped between this tape and the rubber gasket affixed to the ring.

An aluminum bar was suspended over the segment at its approximate center. This bar was leveled as it just touched the top of the segment. By holding the ends of the bar against vertical scales, the height of the segment above the floor could be determined.

Each segment was fitted with a 15.24-cm diameter flexible tube for inflation, and a 1.27-cm diameter plastic valve which was used as a pressure tap. The segment was inflated through the 15.24-cm tube by means of a rheostat-controlled industrial vacuum cleaner. A rubber tube of 1.27-cm i.d. connected the pressure tap to two pressure gages.

A large duct fitting, called a "crown valve", to regulate the flow of air exhausting from the top of the sphere, was taped shut so that no air could escape. The valve was suspended by a cable and counterbalanced by a weight container. As weights were added or removed from the container, the valve could be raised or lowered.

The acceptance criterion of these fittings was no failures within the reinforced area (where duct is joined to sphere) or within 5.08 cm of the reinforced area, when the computed skin stress is 1103×10^6 dyn/cm^2.

When the segment was secured to the floor and inflated enough to just lift it off the floor, it had about a 13.7- to 15.2-meter radius. Thereafter, as pressure was increased, the equivalent sphere radius continued to decrease as the segment rose higher. In other words, while "C" in the adjoining sketch remains constant, "h" is increasing. By knowing C and h, the equivalent sphere radius can be approximated by using tables, if the arc is assumed to be a portion of a sphere.

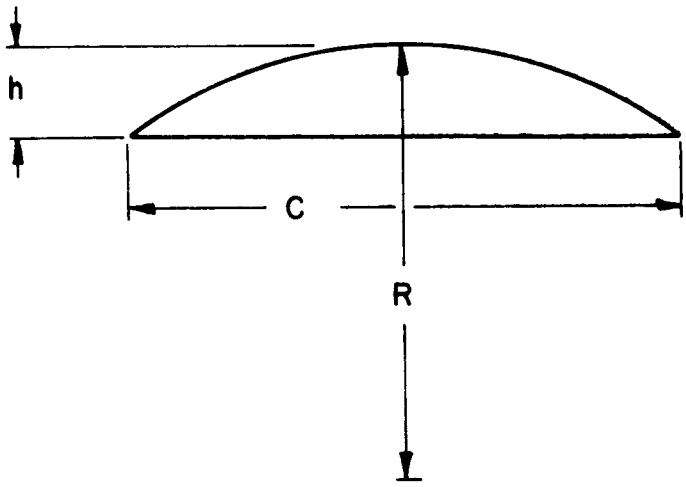

With the sphere radius determined, the skin stress in the segment can be computed from the relationship, $S = pr/2t$. This is the formula for skin stress in a thin-walled sphere, but it also holds true for a segment of a sphere. It is recognized that the segment may not be exactly spherical, therefore the stresses were lower at the top than on the periphery.

Extensometers were placed on the segment skin to obtain a rough measure of skin elongation under pressure. An extensometer is a simple device, which, when taped on a relaxed, unstretched material, permits reading directly the percentage increase in length of the material. The initial relaxed length in this case was 30.48 cm. One extensometer was taped on a seal, one on a gore, and one perpendicular to the first two across one seal. Readings were recorded at each pressure interval.

A black ink mark was placed on several butt joints and seals prior to testing. Any separation or creep of the tape seals would show as a visible line appearing in the ink mark.

The segments were pressurized with increments of 0.5×10^{-3} dyn/cm^2, holding 5 minutes at each level until 2.5×10^{-3} dyn/cm^2 was reached. This

was held for one hour and then the pressure was again increased incrementally by 0.5×10^{-3} dyn/cm^2, holding 5 minutes at each level until rupture occurred.

During the tests, the appearance of the segments was good. The surface of the aluminized PET was extremely reflective and smooth, especially at the higher pressures. All segments reached 1103×10^6 dyn/cm^2 skin stress before rupture. Neither of the two duct segments failed in the direct region of the duct junction.

The seals revealed no signs of any adhesive creep or separation in the butt joint.

The polar cap segment had no ducts attached. A crack in one gore occurred about 46 to 50 cm from the polar cap cut-out at a pressure of 6.5×10^{-3} dyn/cm^2, but went only as far as the edge of the tape on the seal on either side. It occurred where a small hole was observed earlier in the test, and repaired with a small piece of pressure sensitive tape. The segment ruptured at a pressure of 7.5×10^{-3} dyn/cm^2. It proceeded from the initial crack and had enough force to completely sever both inner and outer pole caps. Since the radius was 4.14 m based on 69 cm height, the stress was 1220×10^6 dyn/cm^2. The skin stress at a pressure of 6.48×10^{-3} dyn/cm^2 (at which the crack in the gore occurred) was 1131×10^6 dyn/cm^2.

This side duct segment did not suffer any premature breaks as did the polar cap segments, but burst catastrophically at a pressure of 7×10^{-3} dyn/cm^2 and a height of about 74 cm. This is equivalent to approximately 1100×10^6 dyn/cm^2 skin stress. The burst occurred down the center of a gore.

The north duct segment burst lengthwise in the center of a gore about 46 cm from the duct junction at a pressure of 6.2×10^{-3} dyn/cm^2 and a height of about 69 cm. This is equal to 1020×10^6 dyn/cm^2 skin stress due to internal pressure. At the time of burst, a 72.6 kg upward pull was being exerted on the duct. This upward force added a stress of 175×10^6 dyn/cm^2 to the single-thickness PET immediately surrounding the duct junction.

Since stress = $\frac{\text{upward force}}{(\text{duct reinforcement perimeter})(\text{thickness})}$, a force of 1195×10^6 dyn/cm^2 (1020 + 175) was being exerted in the critical area near the duct fastening.

A slight separation of one of the pleats in the duct fastening was noticed at a pressure of 4.5×10^{-3} dyn/cm^2, but there was no leak and no further separation occurred. The final rupture did not occur near this separation.

All three segments demonstrated a very smooth and reflective surface, from the outer edge right up to the duct junction. This is indicative of proper cutting and fabrication techniques.

The adhesive used in the duct work withstands high peel and shear loads without creep or separation.

The 445×10^6 dyn test line used in the north duct was adequate to retain the hoop stress set up at the duct junction.

The scrim material used as duct reinforcement did not tear or stretch.

The material from which the ducts were fabricated withstood the tests without any indications of separation, bulges, or butt seal separation.

It was concluded from these segment tests that the duct configurations were fully adequate for use on the PAGEOS static inflation test sphere.

Inflation test.—The PAGEOS sphere was erected and inflated by forcing air into the sphere to produce various pressure levels from 48×10^6 dyn/cm^2 (1.13×10^{-3} dyn/cm^2), where the sphere ruptured.

The polar diameter was oriented vertically and the bottom of the sphere was maintained about 3.7 m from the floor. Once inflated, the sphere was maintained in its location by 14 tie-down lines evenly spaced about the sphere.

The internal pressure of the sphere was read directly on two inclined manometers and recorded on a pressure recorder, connected to the sphere by a 18-m long, 1.27-cm i.d., flexible tube. A pressure controlling unit, with a pneumatic output connected to the air delivery system, maintained the proper pressure in the sphere, once reached. A large fan delivered air at room temperature, or slightly warmed, through a duct at the bottom of the sphere. Supplies of helium and carbon dioxide were maintained at the mouth of the fan intake to provide a way of adjusting the lift should the situation require. A valve, situated above the sphere and operable by remote ground control, could be used to allow warm air or helium to pass from the sphere upward through a duct joined to the top of the sphere if excess lift developed. Helium and warm air could be added to the input duct when the sphere became heavy.

A large canopy suspended from the hangar ceiling protected the sphere during the Static Inflation Test.

When the sphere was nearing completion of initial inflation at the SIT, inspection of the sphere skin revealed three holes. Two were small, about 2.5 cm, and the third was about 38 cm long. These holes were attributed to adhesion and carefully patched with metalized PET tape.

Pressure testing was initiated at 48×10^6 dyn/cm^2 skin stress and increased in step-fashion until the sphere burst at 690×10^6 dyn/cm^2. Thereafter, the sphere was investigated at the test site to determine probable causes and areas of initial failure. The suspect areas were cut from the sphere for further study.

Thermocouples were placed outside and inside the sphere. The thermocouples, connected to a 12-channel temperature recorder, gave a continuous picture of the temperature conditions in and around the sphere. The temperature information was used to anticipate the need for added or decreased lift in the sphere.

Sphere diameter: The objective of this test was to determine the equatorial and polar diameter of the test sphere at various pressure levels. It was required that the inflatable spheres be 30.48 meters in diameter ± 0.5 per cent as measured at the static inflation test. The polar diameter and the average equatorial diameter were to be equal within this tolerance at least one time between 48×10^6 and 689.5×10^6 dyn/cm^2 skin stress.

The polar diameter was measured by a 1.27-cm wide, 0.127-mm thick, PET tape which was suspended from the top of the sphere, through the inside, and out the bottom duct of the sphere. A 624-gm weight fastened to the tape at the bottom maintained uniform tension. The polar diameter was the numerical average of the readings of four people who each made independent readings of the tape.

It was found that the 624-gm weight applied to the end of the tape stretched it approximately 2.54 cm in 30.48 meters. Consequently, the polar diameter of the sphere was at all times 2.54 cm greater than the tape indicated.

Eight theodolites, spaced evenly about the sphere, were used to measure the equatorial diameter of the sphere. To provide high visibility location points on the equatorial diameter of the sphere, eight white polyurethane cones with 1.27-cm diameter orange balls at the apex were attached to the equator. Prior to fastening the cones to the test sphere, they were accurately measured from the base to the center of the balls. All theodolite operators were fully qualified operators, being either registered engineers or registered land surveyors.

In computing equatorial diameter, the engineers used a grid coordinate system.

Consider theodolite stations 2 and 3 with coordinates X_2, Y_2, X_3, Y_3, respectively in the diagram below.

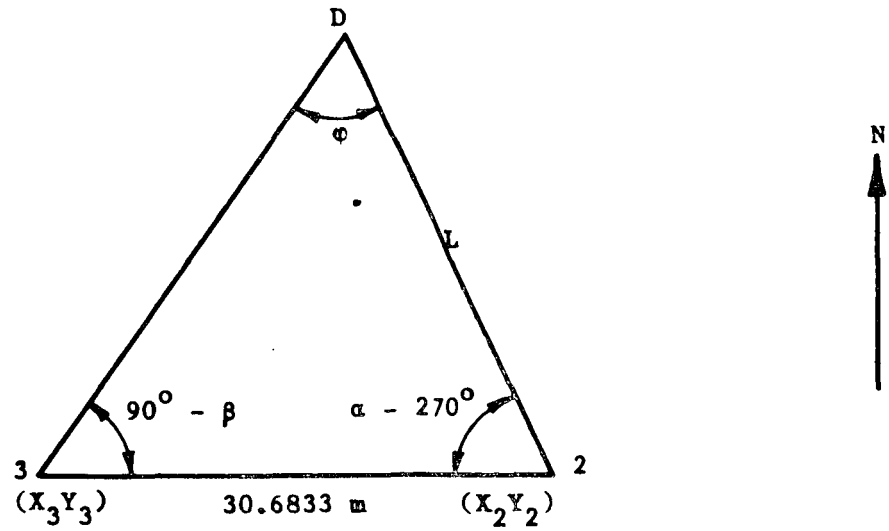

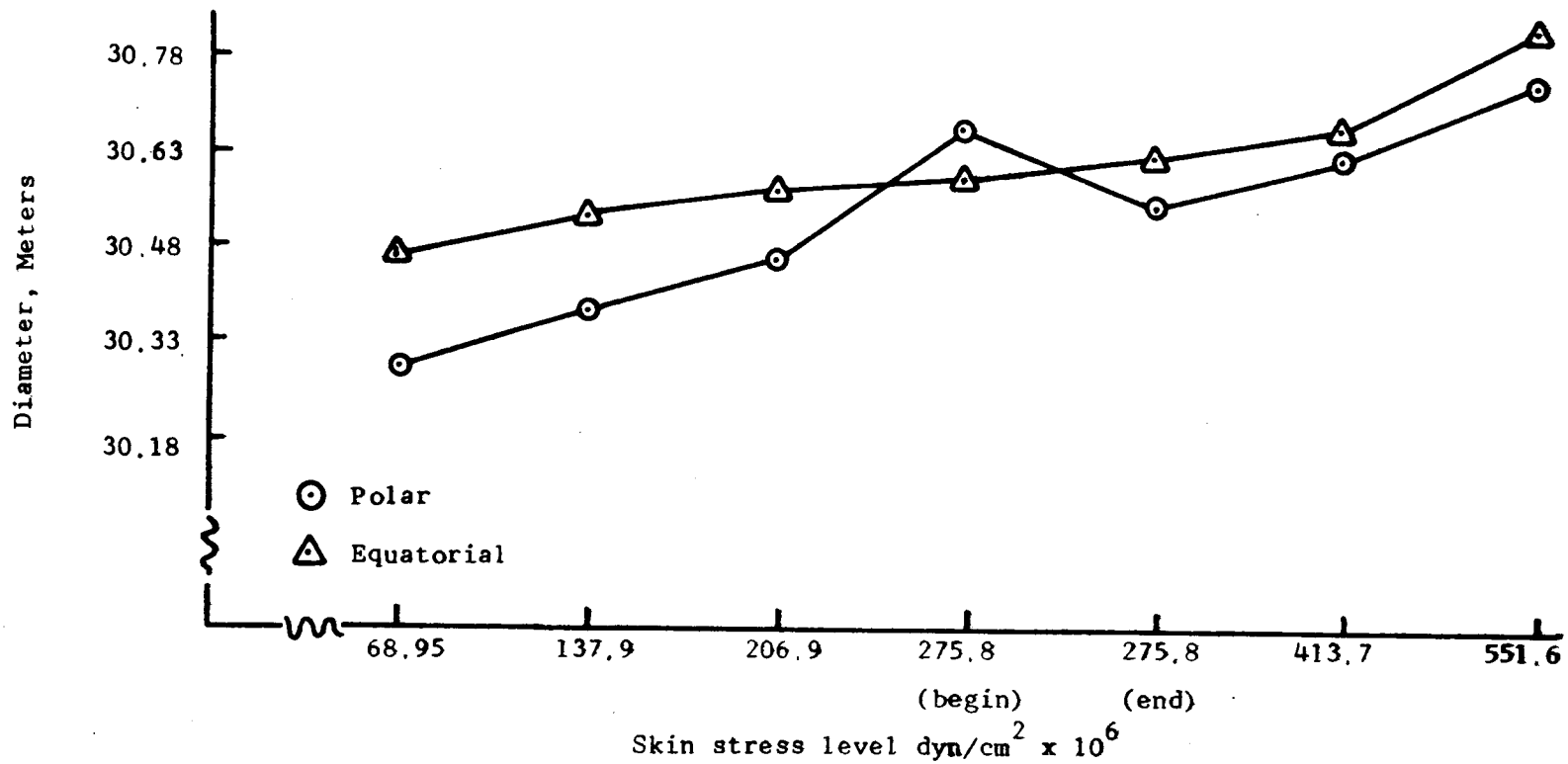

Figure 15.- Equatorial vs. polar diameter.

Each instrument sights on the scribed brass plate of the other instrument. Two looks at three and sets 270° 00' 00" on the angular scale; three looks at two and sets 90° 00' 00" on the angular scale. Two and three each then track cone D, and, on the command given from the control center over telephone headsets, they stop tracking and record the azimuth angle. The azimuth angle of line 2-D in the above sketch is α and the azimuth angle of line 3-D is β. The angle at D then is $\varphi = 180 - (90 - \beta) - (\alpha - 270)$. From the law of sines, the length of line 2-D equals $L = \frac{30.6833 \sin(90-\beta)}{\sin \varphi}$, then, the coordinates of point D on the grid system are $X_D = X_2 - L \sin (360 - \alpha)$, and $Y_D = Y_2 + L \cos (360 - \alpha)$. On the opposite side of the sphere, the coordinates of a second point, H, is simultaneously determined. The diameter, D, is then computed from the coordinates by the equation, Diameter $= \sqrt{(X_D - X_H)^2 + (Y_D - Y_H)^2}$.

A graph (figure 15) illustrates the diameter measurements as computed at each pressure level. The polar diameter was found to be slightly less than the equatorial diameter except at the beginning of the 5-hour 275.8 x 10^6 dyn/cm^2 test. Here, the polar diameter was somewhat greater than the equatorial, indicating that if lines are drawn to connect points, they will cross somewhere before the 275.8 x 10^6 dyn/cm^2 level and within the 30.48 meters $\pm$ 5 per cent desired.

Seam creep: The objective of this test was to ascertain whether or not the single-tape seal permitted any creeping apart of the two gores which were butted together at the center of the seam.

The seam creep, if any, could be detected initially by the appearance of a bright line in the center of the black ink spot which was placed on each butt-joint about 6 m from the south pole. If an indication of creep occurred, the extent of such separation could be determined by placing a calibrated loupe on the ink spot, and measuring the width of the bright line.

Since no seam creep was noted during the test or in the postrupture inspection, it was concluded that sealing procedures, temperatures, and quality of adhesive were satisfactory. Laboratory creep tests (performed at 138 x 10^6 dyn/cm^2 skin stress at 150 C) resulted in no creep and therefore none was expected on the test sphere.

Dc continuity: The objective of the dc continuity check was to determine the effectiveness of the continuity strip located on the sphere polar areas.

A voltmeter with flat, circular brass contacts was applied against the sphere skin. The contacts were made at the south pole area about 61 cm from the duct. At first the contacts were placed in the center of the two gores across whose mutual seam the electrical conductivity was to be measured. It was found, however, that the resistance in most cases was infinite. The contacts were then placed as shown in the sketch below, and more meaningful readings were obtained.

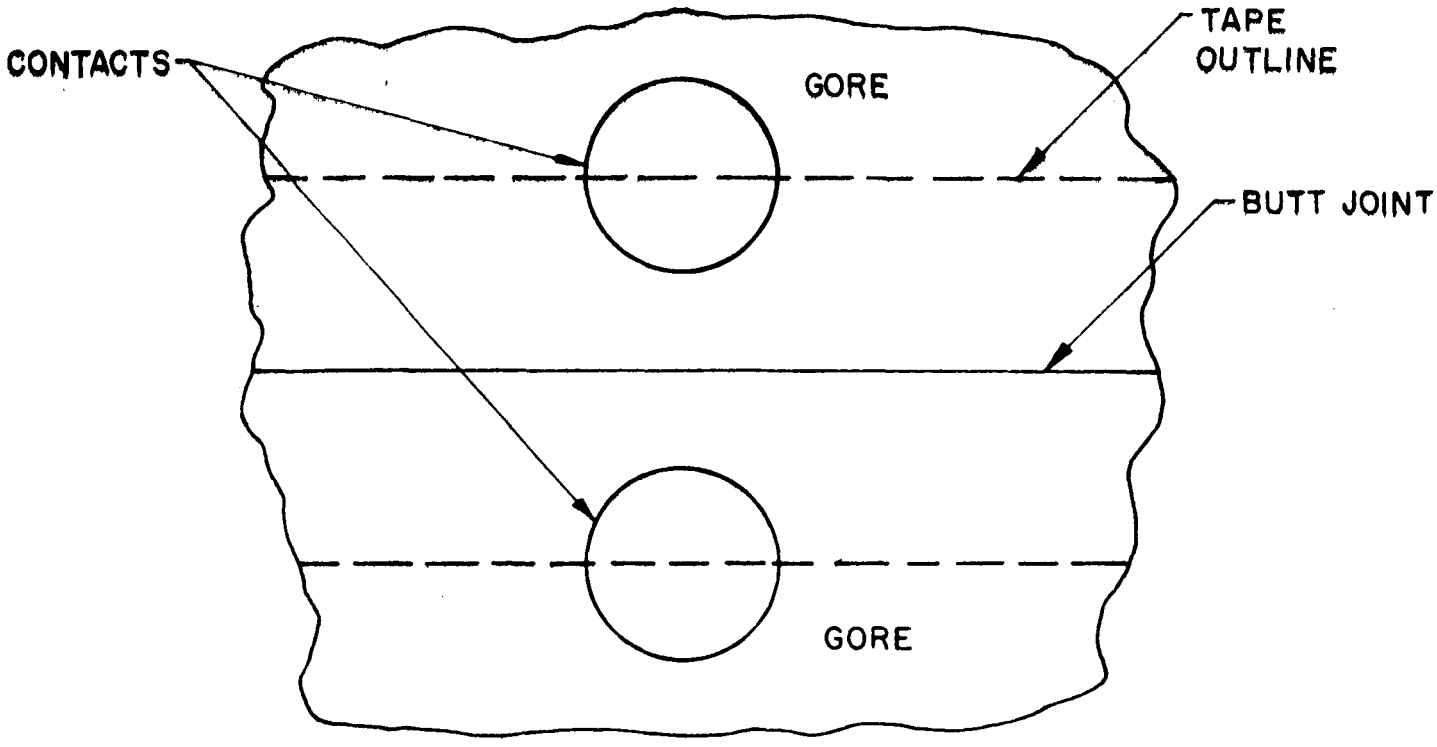

Resistance measurements prior to burst varied from 1 to 200 ohms, but most were in the range of 50 to 100 ohms. As pressure level increased, the average resistance readings seemed generally to decrease. This was probably because the smoother and firmer sphere skin allowed better electrical contact. After rupture of the sphere the resistance was generally higher, in the range of 50 to 300 ohms.

Appearance: The general appearance of the sphere was very good. The tape seals were smooth and even, and not readily detectable from a distance, particularly when the sphere was at the higher pressure levels. A few small wrinkles were evident in the skin at initial inflation and at 48 x 10^6 dyn/cm^2 skin stress. These all disappeared, however, as the pressure was increased to 137.9 x 10^6 dyn/cm^2.

A ring of relatively loose material was evident on the top side of the sphere. The ring was about 3.048 meters in diameter and concentric with the north polar duct. This dictated a minor tooling adjustment.

Sphere rupture: The sphere burst after being at 690 x 10^6 dyn/cm^2 skin stress for approximately 5 minutes. It is believed that the point of initial burst was in seal 24, between gore 24 and 25. The evidence indicated that the rupture was caused by a small tuck or underlap of a gore just under the edge of the tape.

TABLE 3.- TEST ACCEPTANCE CRITERIA

TEST	ACCEPTANCE CRITERIA	SAMPLE SIZE	TEST EQUIPMENT
Material			
Thickness	0.0127 ± 0.00127 mm	2.5 × 20.1 cm	Thickness gage
Tensile Strength	1241×10^6 dyn/cm^2	2.5 × 20.1 cm	Tensile strength tester
Tensile Impact	4.21×10^6 dyn-cm	2.5 × 20.1 cm	Tensile impact tester
Resistivity	less than 1.0 ohm/square	2.5 × 20.1 cm	Resistance gage
Aluminum Adhesion	no metalizing transfer	10.2 × 122.0 cm	Pressure sensitive tape
Reflectance		5.0 × 5.0 cm	Spectrophotometer
Total Diffused Component	83.0% minimum and 90.0% max. less than 7.0%		
Hot-Wheel Adhesion	no tear*	5.0 × 126.0 cm	Tensile strength tester
PET Adhesion	no tear**	5.0 × 126.0 cm	Tensile strength tester
Seal			
Thermal Shock	1241×10^6 dyn/cm^2 psi minimum	2.5 × 22.8 cm	Thermal shock machine and tensile strength tester
Thermal Flexure	1241×10^6 dyn/cm^2 minimum	2.5 × 22.8 cm	Thermal shock machine and tensile strength tester
Seal Peel	0.0232 Kg/cm minimum or tearing of material	2.5 × 22.8 cm	Tensile strength tester
Seam Creep	5.08 mm maximum	2.5 × 22.8	Heated over w/tension clamp and machinists scale
Repair			
Seal Peel	0.0228×10^6 dyn/cm minimum or tearing of material	2.5 × 22.8 cm	Tensile strength tester
Tape			
Thickness (PET only)	0.0127 ± 0.00127 mm	2.5 × 20.1 cm	Thickness gage
Tensile Strength	1241×10^6 dyn/cm^2	2.5 × 20.1 cm	Tensile strength machine
Peel (bond strength)	0.0228×10^6 dyn/cm minimum or material tearing	2.5 × 22.8 cm	Tensile strength machine

*5.8×10^3 dyn/cm maximum and no tear for Spheres 4 and 5
**15.4×10^3 dyn/cm maximum and no tear for Spheres 4 and 5

ACCEPTANCE TESTING

A test program was instituted to insure high reliability and structural integrity of all the components used in the manufacture of the spheres, as well as their conformance to the design and functional requirements, and to measure a series of critical characteristics for the various components. The testing procedures simulated the methods, tooling, and design utilized in the normal production routine. Table 3 identifies characteristics and their respective acceptance criteria. Test results of variables characteristics including computed sample means and standard deviations are unbiased estimates of the population means and standard deviation. Table 4 shows a computed sample mean and standard deviation for each critical characteristic by sphere number. Grand calculated means and standard deviations are also shown. These values are estimates of the characteristic parameters of the PAGEOS material and seals for all six spheres.

Manufacturing repairs are tabulated by sphere number in Table 5 and are categorized by material and seals.

In the case of attributes characteristics, the fractions of failure (fraction defectives) are calculated for each sphere and the results appear in Table 6.

TABLE 4.- VARIABLE CHARACTERISTICS TEST RESULTS (Metalized PET)

CHARACTERISTIC	SPHERE NUMBER	SAMPLE MEAN ($\bar{x}$)	SAMPLE STANDARD DEVIATION (σ)	THREE STANDARD DEVIATION LIMITS LOWER ($\bar{x}-3\sigma$)	UPPER ($\bar{x}+3\sigma$)
Tensile Strength ($dyn/cm^2 \times 10^6$)	1	1924	290	1054	2794
	2	1841	276	1013	2669
	3	1751	241	1028	2474
	4	1806	290	936	2676
	5	1848	303	939	2757
	6	1848	276	1020	2676
	(1-6)	1834	298	946	2722
Tensile Impact* ($dyn\text{-}cm \times 10^6$)	1	9.91	3.26	0.13	19.69
	2	7.36	1.73	2.17	12.55
	3	8.80	1.64	3.88	13.72
	4	9.18	2.20	2.58	15.78
	5	9.81	2.77	1.50	18.12
	6	9.32	2.54	1.70	16.94
	(1-6)	9.06	2.33	2.07	16.05

TABLE 4.- VARIABLE CHARACTERISTICS TESTS RESULTS (Metalized PET) (Concluded)

CHARACTERISTIC	SPHERE NUMBER	SAMPLE MEAN ($\bar{x}$)	SAMPLE STANDARD DEVIATION (σ)	THREE STANDARD DEVIATION LIMITS LOWER ($\bar{x}-3\sigma$)	UPPER ($\bar{x}+3\sigma$)
Reflectance (%)	1	89.1	0.4	87.9	90.3
	2	89.1	0.6	87.3	90.0
	3	89.1	1.1	85.8	92.4
	4	89.3	1.3	85.4	93.2
	5	89.0	0.4	87.8	90.2
	6	89.3	1.0	86.3	92.3
	(1-6)	89.2	1.1	86.1	92.5
Thermal Shock ($dyn/cm^2 \times 10^6$)	1	1972	283	1131	2821
	2	1820	255	1055	2585
	3	1765	221	1102	2428
	4	1793	200	1193	2393
	5	1875	207	1254	2496
	6	1793	186	1235	2351
	(1-6)	1841	228	1157	2525
Thermal Flexure ($dyn/cm^2 \times 10^6$)	1	1972	214	1330	2614
	2	1800	310	870	2730
	3	1765	214	1123	2407
	4	1813	214	1171	2455
	5	1875	179	1338	2412
	6	1806	234	1104	2508
	(1-6)	1841	234	1139	2543
Seam Creep (mm)	1	0.229	0.102	0.000	0.535
	2	0.152	0.076	0.000	0.380
	3	0.076	0.051	0.000	0.229
	4	0.229	0.127	0.000	0.610
	5	0.203	0.177	0.000	0.734
	6	0.279	0.152	0.000	0.735
	(1-6)	0.203	0.152	0.000	0.659

*The probability distribution of Tensile Impact is not normal.

TABLE 5.

MANUFACTURING REPAIR RESULTS

SPHERE NUMBER	MATERIAL REPAIR QUANTITY	SEAL REPAIR QUANTITY
1*	32	26
2	25	123
3	4	1
4	9	0
5**	5	2
6**	8	1
(1-6)	82	153

* The inflation system was not installed, although extra operations existed to install duct work for the Static Inflation Test.

** Neither the final seal nor the inflation system was installed.

TABLE 6.

ATTRIBUTE CHARACTERISTICS TEST RESULTS

CHARACTERISTIC	SPHERE NUMBER	FRACTION DEFECTIVE	SAMPLE SIZE
Canister Simulation Adhesion	1	*	*
	2	.000	522
	3	.000	531
	4	.011	528
	5	.000	405
	6	.000	387
	(2-6)	.003	2373
Sealing Wheel Adhesion	1	*	*
	2	.000	522
	3	.012	495
	4	.011	525
	5	.014	420
	6	.003	396
	(2-6)	.008	2358
Aluminum Adhesion	1	.000	636
	2	.000	522
	3	.000	531
	4	.028	537
	5	.060	453
	6	.008	396
	(1-6)	.015	3075
Seam Peel	1	.012	166
	2	.014	168
	3	.000	168
	4	.000	170
	5	.000	168
	6	.000	168
	(1-6)	.003	1008

*This characteristic was not tested during Sphere 1 fabrication.

Material Testing

Test samples of material used in the manufacture of the PAGEOS spheres were taken from both ends of the gore material. Usually the "end" sample of one gore blank was the same as the "start" sample of the following gore blank. If any of the test specimens failed, both gore blanks were rejected. Material failure on any test resulted in rejection. Test specimens were removed and marked. When reject material occurred between gore blanks, specimens were taken at the beginning and end of the reject material. The results of these sample tests applied only to the adjacent gore.

Seal Testing

Samples of seals were taken at both the "start" and "end" of a seal to more closely test the quality of the seal. The failure of the seam creep test resulted in the installation of a bitape seal (a reinforcing strip of tape applied to the underside of the seal). Failure of any other test was cause for removal of the gore.

During the evaluation of the seam peel test, the adequacy of the back-up sealing wheel was evaluated. A seal was made around the entire circumference of the wheel resulting in a sample seal about 3.6 meters long. This was cut into 20 cm lengths and each piece tested for tensile strength after thermal shock. Since there were no failures, it was concluded that the sealing wheel was uniform around its entire circumference.

Repair Testing

Where repairs were necessary, specimens of the repair were taken. Only the seam peel test was conducted, as the tape used in the repair had been previously tested. If, however, several consecutive repairs were made, only one test sample was taken between repairs, the failure of that sample to meet acceptance criteria was cause for rejection of repairs made before and after the sample.

Tape Testing

The tape used in either the seals or repairs was sampled and tested before the material was used. The thickness was measured along the length of the strip. Failure of any sample to meet acceptance criteria caused rejection of that roll of tape.

RELIABILITY

Before developing the Reliability Goal it is necessary to discuss the "state-of-the-art" of reliability prediction with respect to inflatable spheres. The classic approach to reliability, that is to undertake a long range program to test a quantity of spheres to establish the reliability by a statistical method, is not feasible. However, Echo I and Echo II spheres have demonstrated that such a balloon system is feasible, and that rigid quality control, reliability requirements, and a thorough material testing program can achieve high reliability.

The classic approach to reliability requires testing samples of significant size to determine failure rates. For many items there are published government and industry failure rates for various components. There are no established failure rate data for inflatable sphere components.

Data used to develop reliability predictions for PAGEOS inflatable spheres will be those data developed from the acceptance tests.

Failure Mode, Effect, and Criticality Analysis

The PAGEOS project mission was to place a 30.48 m diameter sphere into a near polar orbit at a distance of 4,250 kilometers. The sphere (satellite) is a specular, solar reflector which is being used for a period of about five years to determine the size and shape of the earth, and the position of land masses on the earth. The requirements of this mission were as follows:

1. The satellite will deploy (inflate) in the described environment.

2. The satellite will remain intact during deployment and pressure decay.

3. The reflectance of the satellite will meet the required specular level during the operational period.

Figures 16 and 17 describe the flight profile of the PAGEOS satellite. The operational flight of the satellite consists of four stages as shown in figure 18. This document considers only those stages labeled 1, 2, and 3. They are as follows:

Time Stage 1 - Inflation (1/2 hour)

Time Stage 2 - Pressure Decay (2 weeks)

Time Stage 3 - Orbit (5 years)

In consideration of these time stages as they relate to the requirements of the mission, an analysis in Table 7 identifies potential failures, their

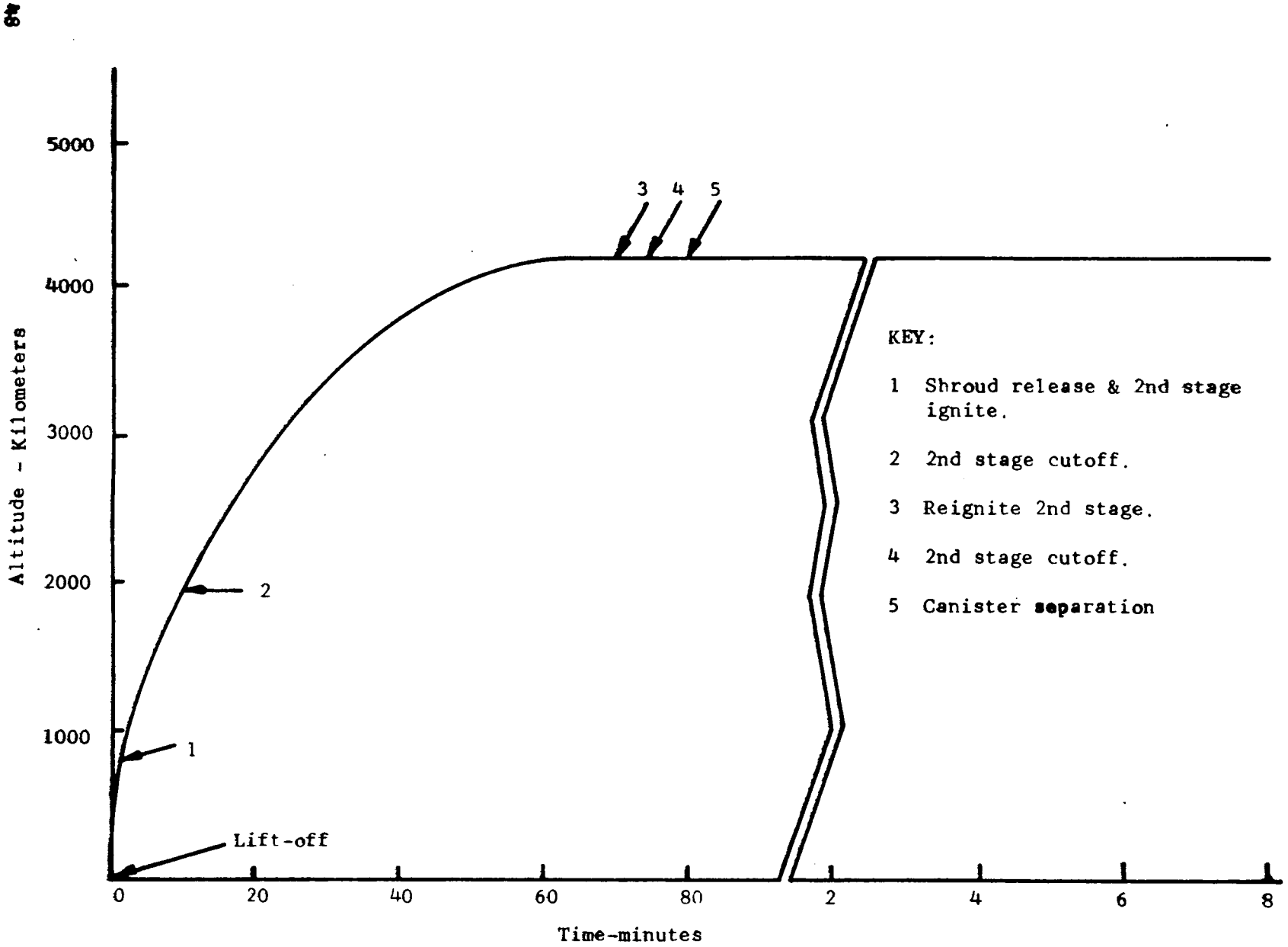

Figure 16.- Flight profile of PAGEOS satellite.

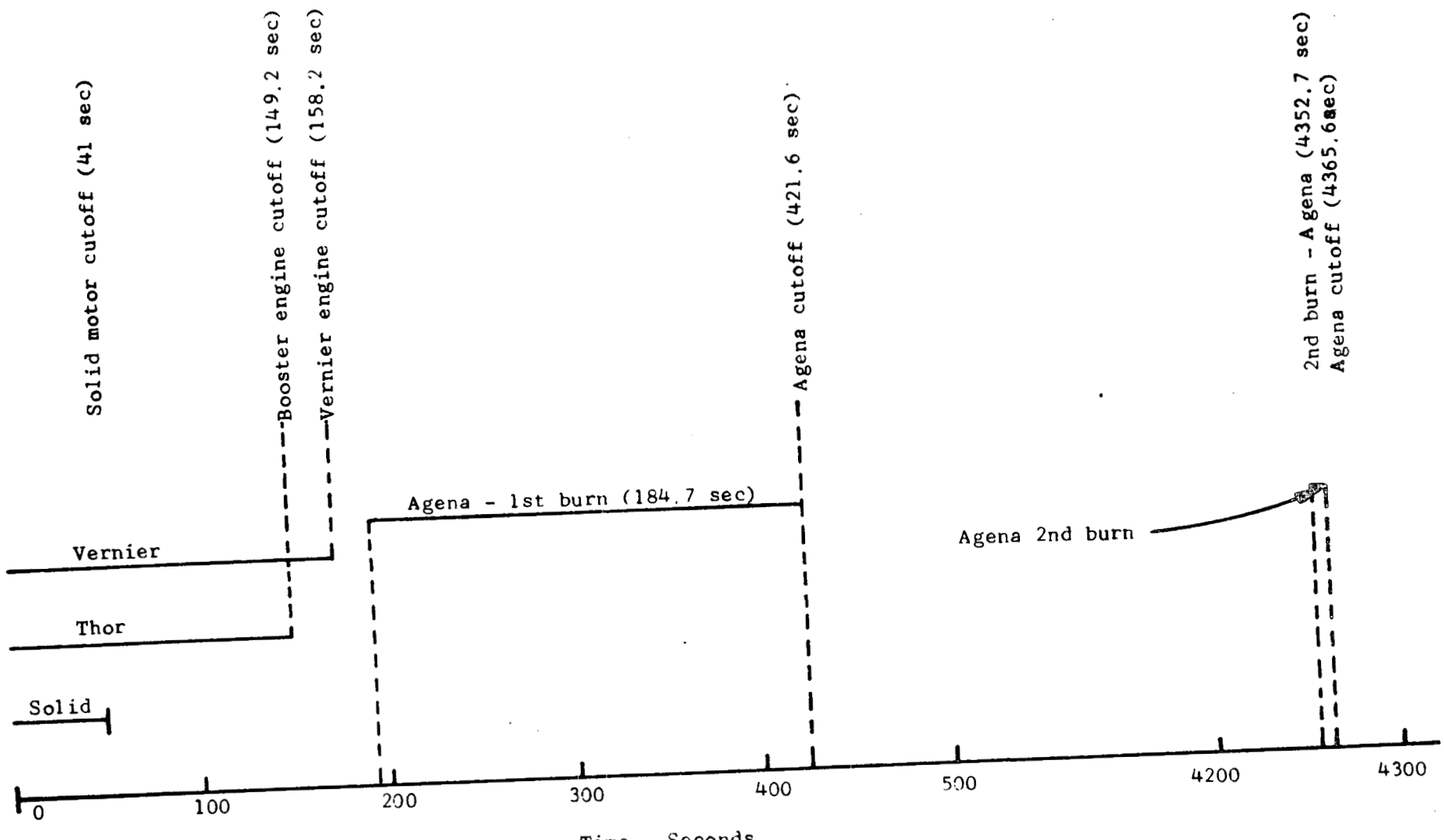

Figure 17.- Engine schedule PAGEOS satellite.

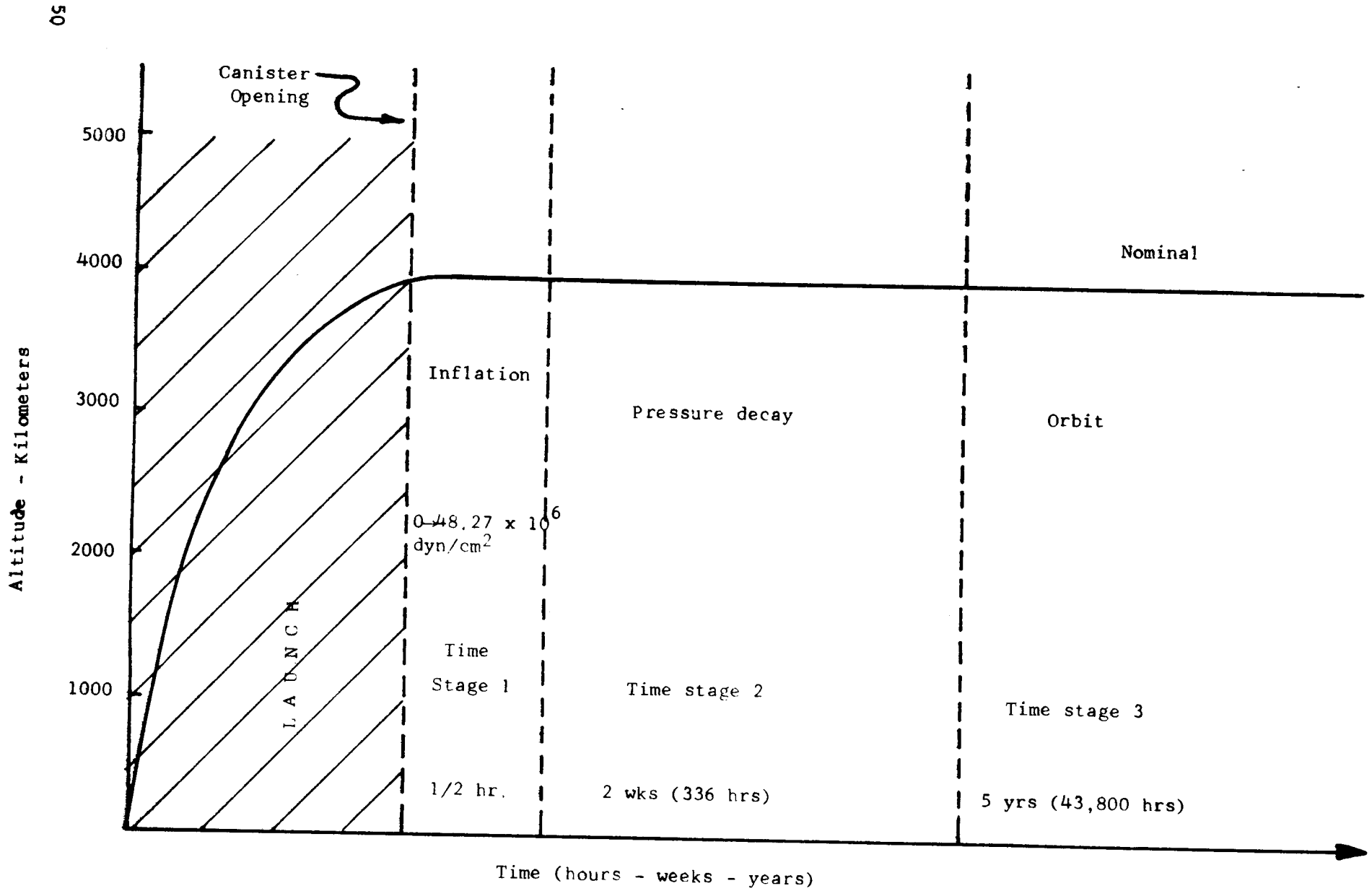

Figure 18.- Operational flight stages of PAGEOS satellite.

TABLE 7.

STAGE	FAILURE CRITICAL (Potential Failures)	FAILURE EFFECT	FAILURE MODE
1. Inflation	1. Burst	Mission Failure	1. Structural deficiency in component a. Gore b. Seal c. Outer Pole Cap d. Inner Pole Cap e. Outer Cap Seal f. Inner Cap Seal g. Final Seal 2. Entangled folds or disarray of folds causing severe stress areas 3. Puncture or tear from fragment of canister or rocket 4. Improper distribution of inflation compounds 5. Improper mixture of inflation compounds 6. Excessive amount of inflation compounds causing over-expansion 7. Excessive heat causing over-expansion 8. Trapped residual air or moisture

TABLE 7. (Continued)

STAGE	FAILURE CRITICAL (Potential Failures)	FAILURE EFFECT	FAILURE MODE
1. Inflation (continued)	2. Failure to inflate	Mission Failure	1. Insufficient amount of inflation powder
			2. Severe tear causing rapid gas leakage due to structural deficiency
			3. Improper mixture of inflation powder
			4. Seal ("O" ring) from canister restraining inflation
	3. Under-inflation	Mission Failure	1. Insufficient amount of inflation powder
			2. Tear(s) or puncture(s) causing gas leakage due to structural deficiency
			3. Improper mixture of inflation compounds
			4. Entangled tip portion of sphere (knot)
			5. Seal from canister restraining inflation

TABLE 7. (Concluded)

STAGE	FAILURE CRITICAL (Potential Failures)	FAILURE EFFECT	FAILURE MODE
2. Pressure Delay	1. Burst	Mission Failure	1. Weakening during inflation causing eventual breakdown of the sphere
			2. Massive meteoroid bombardment
			3. Excessive expansion during inflation causing severe stress
			4. uv degradation of material while sphere is pressurized
3. Orbit	1. Total Reflectivity Loss	Mission Failure	1. Total degradation of reflective surface due to space environment
			2. Massive meteoroid bombardment
	2. Partial Reflectivity Loss	Partial Mission Success	1. Localized meteoroid bombardment
			2. Puncture or tear in material
			3. Seal separation
			4. Partial degradation of reflectance surface due to space environment
			5. Excess spin rotation resulting in misshaped sphere

effects on mission success, and the associated modes of failure. These factors were considered in design specifications, fabrication procedures, and tooling. The primary objectives of this analysis, then, is to determine potential system failures under anticipated conditions, i.e. the space environment, and to establish a reliability goal for the system and its components.

Reliability Goal Establishment and Apportionment

A reliability goal for the PAGEOS Inflatable Sphere Assembly was chosen to be .9600.

The operational flight of the PAGEOS satellite is composed of four significant events occurring at four stages. These are shown in Figure 18. This analysis is restricted to the last three labeled time stages 1, 2, and 3.

Letting Event A be successful inflation; Event B, successful pressure decay; and Event C, successful orbit; then P(A) is the conditional probability of Event A; P(B/A), the conditional probability of Event B given A; P(C/B, A), the conditional probability of Event C, given Events B and A; and P(A, B, C) is the joint probability of Events A, B, and C. Then, the expression for P(A, B, C) is

$$P(A, B, C) = P(C/B, A) \cdot P(B/A) \cdot P(A). \tag{8}$$

Let R_i be the probability of success (reliability) for the i^{th} time stage. The expressions defining R_i for time stages i = 1, 2, and 3 are

$$R_1 = P(A) \tag{9}$$

$$R_2 = P(B/A), \tag{10}$$

and

$$R_3 = P(C/B, A). \tag{11}$$

The system reliability, then, is

$$R_{system} = R_1 \cdot R_2 \cdot R_3. \tag{12}$$

Wherever survival time is of concern, the exponential distribution is assumed to hold. In the case of survival of cycles of operation, the Poisson distribution is assumed to apply. The reliability expression for the i^{th} time stage then becomes

$$R_i = \exp - \lambda_i t_i \tag{13}$$

where λ_i is the mean failure rate for the i^{th} time stage in failures per unit time and t_i is the operational time of the i^{th} stage; or

$$R_i = \exp - \lambda_i C_i \qquad (14)$$

where λ_i is the mean failure rate for the i^{th} time stage in failures per cycle and C_i is the number of operating cycles of the i^{th} time stage.

Equation (14) will be used for stage i = 1 and equation 13 for stages i = 2 and 3 since the concern in stage i = 1 is the survival of operating cycles and survival time is of concern in stages i = 2 and 3 (see figure 18).

Substituting equations (13) and (14) into equation (12) determines

$$R_{system} = \exp - (\lambda_1 C_1 + \lambda_2 t_2 + \lambda_3 t_3). \qquad (15)$$

The reliability goal for the system (.9600) must now be apportioned among the three time stages (reliability phases).

For the time stages i = 1, 2, and 3, the expressions for the expected number of failures are $\lambda_1 C_1$, $\lambda_2 t_2$, and $\lambda_3 t_3$, respectively.

Since no information is available which provides failure rate data for inflatable spheres of this type, it is necessary to use engineering judgment in selecting a scale which considers failure and success based on previous experience. If the time stage breakdown of the PAGEOS sphere as shown in Figure 18 is examined and compared with experience (Echo I and II), it is seen that in time stage 3 the conditions are less severe than in stages 1 and 2, and failure is unlikely if the sphere is successful in stages 1 and 2.

In order to solve for stage reliabilities (R_1, R_2, and R_3) it is necessary to express each expected number of failures in terms of a common expected number of failures. Identifying these for time stages i = 1, 2, and 3, we obtain

$$\lambda_1 C_1 = w_1 (\lambda_3 t_3), \qquad (16)$$

$$\lambda_2 t_2 = w_2 (\lambda_3 t_3), \qquad (17)$$

and

$$\lambda_3 t_3 = w_3 (\lambda_3 t_3), \qquad (18)$$

respectively, where w_1, w_2, and w_3 are weights on an arbitrary scale of 1 to 100, and are 99, 9 and 1 respectively. These are based on engineering judgment and previous experience. The common expected number of failures is chosen to be $\lambda_3 t_3$.

Entering these weights in equations (16), (17), and (18), and these equations into equation (15) $\lambda_3 t_3$ is found to be 3.745×10^{-4}. Entering this value in equations (16), (17), and (18), the expected numbers of failures are found as

$$\lambda_1 C_1 = 370.755 \times 10^{-4}$$

$$\lambda_2 t_2 = 33.705 \times 10^{-4},$$

and

$$\lambda_3 t_3 = 3.745 \times 10^{-4}.$$

Solving equations (13) and (14) determines R_1 as .9636, R_2 as .9966, and R_3 as .9996. The stage failure rates (λ_1, λ_2, and λ_3) can then be found by equations 9, 10, and 11, respectively. These are

$$\lambda_1 = .0371 \text{ failures per cycle},$$

$$\lambda_2 = 1.00 \times 10^{-5} \text{ failures per hour},$$

and

$$\lambda_3 = 8.57 \times 10^{-9} \text{ failures per hour}.$$

Having apportioned the system reliability into the three time stages and established the failure rate for each stage, the reliability can be apportioned to the component parts in each stage.

Time stage 1.—The general expression for reliability of stage 1 is

$$R_1 = \exp - C_1 \sum_{j=1}^{n_1} k_j \lambda_{1j} \qquad (19)$$

where

λ_{1j} = failure rate for component j in time stage i = 1,

k_j = quantity of component j applicable to time stage i = 1,

and

n_1 = number of independent components in time stage i = 1 (j = 1, 2, ..., n_1) .

In order to apportion component reliabilities (R_{11}, R_{12}, •••, R_{1j}, •••, R_{1n_1}) it, again, becomes necessary to express each in terms of a common expected number of failures. Consider the common expression to be that of component $j = 1$ or $\lambda_{11}C_1$. Since $C_1 = 1$, $\lambda_{1j}C_1$ becomes λ_{1j} for computation purposes. The failure rate λ_{1j} for $j = 1, 2, \bullet\bullet\bullet, n_1$, then is

$$\lambda_{1j} = w_{1j}\lambda_{11}, \tag{20}$$

expressed in terms of λ_{11} where w_{1j} is a weight for component j considering time stage $i = 1$ selected on the basis of engineering judgment considering an arbitrary scale of 1 to 10. Substituting equation (20) into equation (19) results in

$$R_1 = \exp - \lambda_{11}C_1 \sum_{j=1}^{n_1} k_j w_{1j} . \tag{21}$$

Table 7 identifies the components applicable to stage $i = 1$ and their respective quantities and weights. From Table 8 $n_1 = 8$ and

$$\sum_{j=1}^{n_1} k_j w_{1j} = 178.$$

Using these values in equation 14 where $C_1 = 1$ and $R_1 = .9636$ (previously determined), determines $\lambda_{11} = 2.08 \times 10^{-4}$ failures per cycle. Solving equation (20) for the balance of the component failure rates $\lambda_{12} = \lambda_{13} = \bullet\bullet\bullet = \lambda_{17} = 2.08 \times 10^{-4}$ and $\lambda_{18} = 4.16 \times 10^{-4}$, are found all expressed in terms of failures per cycle.

Having determined the failure rate for each of the components applicable to stage $i = 1$, component reliabilities can be apportioned by the expression

$$R_{1j} = \exp - k_j C_1 \lambda_{1j}. \tag{22}$$

Solving for R_{1j} for $j = 1, 2, \bullet\bullet\bullet, 8$, the following are obtained:

$$R_{11} = .9827$$

$$R_{12} = .9829$$

$$R_{13} = .9996$$

$$R_{14} = .9996$$

TABLE 8.

Stage 1 Components and Their Detail

i	Component	k_j	w_{1j}	$k_j w_{1j}$
1	Gore	84	1	84
2	Seal	83	1	83
3	Outer pole cap	2	1	2
4	Inner pole cap	2	1	2
5	Outer cap seal	2	1	2
6	Inner cap seal	2	1	2
7	Final seal	1	1	1
8	Inflatants	1	2	2

$n_1 = 8$ $\qquad \sum_{j=1}^{8} k_j w_{1j} = 178$

$$R_{15} = .9996$$

$$R_{16} = .9996$$

$$R_{17} = .9998$$

$$R_{18} = .9996 .$$

Time stage 2.—The general expression for reliability of stage 2 is

$$R_2 = \exp - t_2 \sum_{j=1}^{n_2} k_j \lambda_{2j} \qquad (23)$$

where

λ_{2j} = failure rate for component j in time stage i = 2,

k_j = quantity of component j in time stage i = 2,

and

n_2 = number of independent components in time stage i = 2 ($j = 1, 2, \cdots, n_2$).

Following the same pattern as that developed for stage i = 1, component reliabilities can be apportioned as shown in Table 9.

TABLE 9:- STAGE 2 COMPONENTS AND THEIR DETAIL

j	Component	k_j	w_{2j}	$k_j w_{2j}$
1	Gore	84	1	84
2	Seal	83	1	83
3	Outer pole cap	2	1	2
4	Inner pole cap	2	1	2
5	Outer pole cap	2	1	2
6	Final seal	2	1	2
7	Inflatants	1	1	1
			n_2	
$n_2 = 7$			$\sum_{j=1} k_j w_{2j} = 176$	

The reliability for time stage i = 2 in terms of common failure rate, λ_{21} is

$$R_2 = \exp - \lambda_{21} t_2 \sum_{j=1}^{n_2} k_j w_{2j} \qquad (24)$$

Substituting the values of Table 8 in equation (24) since t_2 and R_2 are known, determines $\lambda_{21} = 5.70 \times 10^{-8}$ failures per hour.

Having determined the failure rate for each of the components applicable to stage i = 2, the component reliabilities can determined by equation (25)

$$R_{2j} = \exp - k_j t_{2j} \qquad (25)$$

These are shown below.

$$R_{21} = .9984$$

$$R_{22} = .9984$$

$$R_{23} = .99996$$

$$R_{24} = .99996$$

$$R_{25} = .99996$$

$$R_{26} = .99998.$$

Time stage 3.—It is assumed that if the sphere is successful in stages 1 and 2, the only consideration in stage 3 is that of reflectance over the five year period. Echo I suggests that once successful orbit and inflation are achieved the balance of the mission is readily achieved. If no structural stresses are present in stage 3, the only consideration becomes reflectance. Echo I data further suggest that the space environment does not significantly affect reflectance properties beyond that necessary for a successful mission.

In apportioning the stage reliability into component reliabilities considering reflectance only, the applicable components are seen to be the gore ($j = 1$) and the outer pole cap ($j = 3$). The reliability for time stage $i = 3$, then, can be expressed as

$$R_3 = \exp - t_3 (k_1 \lambda_{31} + k_3 \lambda_{33}). \tag{26}$$

Weighting in the same manner as in previous time stages results in an expression for component j in terms of λ_{33} as

$$\lambda_{3j} = w_{3j} \lambda_{33} . \tag{27}$$

Substituting equation (27) into equation (26), we obtain

$$R_3 = \exp - t_3 (k_1 w_{31} \lambda_{33} + k_3 w_{33} \lambda_{33}). \tag{28}$$

The weights w_{31} and w_{33} are 99 and 1, respectively, determined by engineering judgment. Substituting into equation (28) where R_3, t_3, k_1, and k_3 are known determines λ_{33} as 1.10×10^{-12} failures per hour, and solving for λ_{31} by equation 20 determines λ_{31} as 1.09×10^{-10} failures per hour.

Having determined the failure rates applicable to stage $i = 3$, component reliabilities can be apportioned by the expression

$$R_{3j} = \exp - k_j t_3 \lambda_{3j} \tag{29}$$

Solving for R_{3j} for $j = 1$ and 3, determines R_{31} as .9996 and R_{33} as .999999.

The reliability block diagram which follows (figure 19) shows an analysis of reliability stages and components.

Reliability Prediction

The purpose of this section is to show the mathematical technique for reliability prediction of PAGEOS Inflatable Sphere Assemblies.

Since the classic approach to reliability prediction cannot be used, the development must be made utilizing acceptance tests.

The development of this model takes into consideration the conditions stated in the reliability goal establishment. In particular, the probability development is the model used for combining the reliabilities in the order of time stages. For example, any reliability estimate dealing with time stage 2 is conditional upon success in time stage 1.

Within the framework established in the previous section, the predictions are made for components based on the data obtained from variables testing, attributes testing, and manufacturing defect evaluation. The following paragraphs show the mathematical development which leads to component time-stage reliability and ultimately to a reliability prediction for the PAGEOS sphere assembly.

Testing by variables.—Consider a homogeneous component j where the variable characteristic v is tested and the resulting random variable x_v follows a normal probability distribution with a mean of μ_v and standard deviation of σ_v. If the variable is tested in a specimen size s_v by a random sample of size N_v, the sample mean $\bar{x}_v$ and sample standard deviation sd_v can be computed.

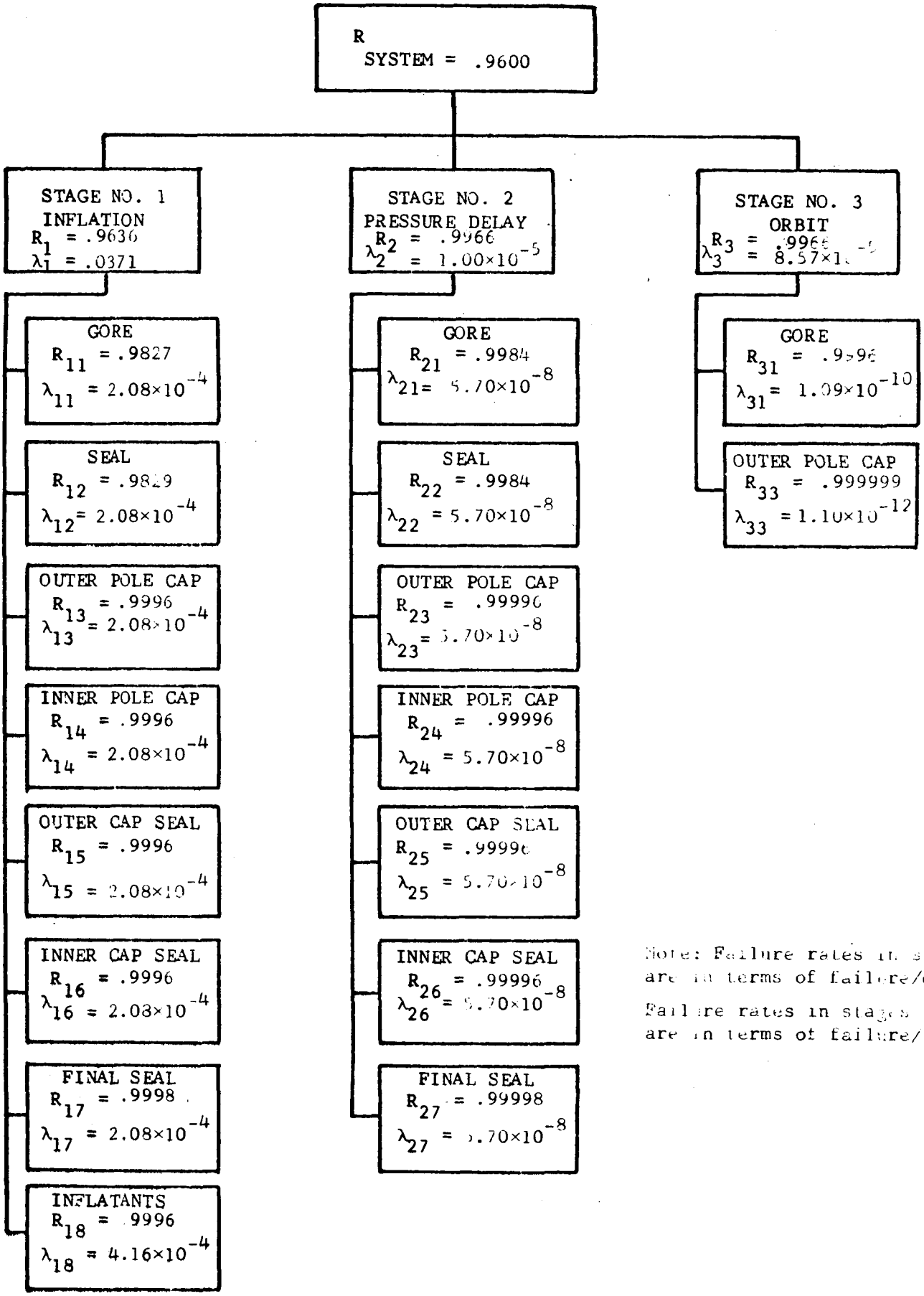

Figure 19.-Reliability goal block diagram.

Let F_{iv} be a maximum or minimum value* of x_v for a specimen size s_v which will result in mission success in time stage i. The characteristic v shall have either a minimum or maximum F_{iv}, but shall not have both. A single specimen having a value less than the minimum F_{iv} or greater than the maximum F_{iv} will cause the mission to fail. For stage i, let P'_{iv} be the fraction* of specimens whose values are less than or greater than F_{iv}, whichever is applicable, and f'_{iv} be the absolute difference between μ_v and F_{iv} in terms of standard deviations.

To estimate P'_{iv} when F_{iv} is a lower limit, we can use the fact that $(s_v - \mu_v)/\sigma_v$ is a standardized normal variable with mean of zero and standard deviation of one. Hence, letting $\Phi(Y)$ denote the standard normal cumulative distribution function, we can write for large values of N_v,

$$P_{iv} = \Phi\left(\frac{F_{iv}-\bar{x}_v}{sd_v}\right) \approx \Phi\left(\frac{F_{iv}-\mu_v}{\sigma_v}\right) = P'_{iv} \qquad (30)$$

When F_{iv} is an upper limit the corresponding estimate of P_{iv} is

$$P_{iv} = 1 - \Phi\left(\frac{F_{iv}-\bar{x}_v}{sd_v}\right) \approx 1 - \Phi\left(\frac{F_{iv}-\mu_v}{\sigma_v}\right) = P'_{iv} . \qquad (31)$$

To cover both conditions with a single table, we can estimate f'_{iv} by the expression

$$f_{iv} = \left|\frac{F_{iv}-\bar{x}_v}{sd_v}\right| \qquad (32)$$

and can read P_{iv} from a one-tail table of the standardized normal distribution.

If the component j is of size S_j, it follows that there are S_j/s_v specimens of size s_v in component j. The estimated number of failures, then, is $(S_j/s_v)P_{iv}$. Assuming that the number of failures follows a Poisson distribution, the reliability**, VR_{ijv}, for component j in stage i, based on variable characteristic v, can be expressed as

$$VR_{ijv} = \exp -\left(S_j/s_v\right)\left(P_{iv}\right) . \qquad (33)$$

* All definitions and estimates in this section that are indexed by i (with i greater than 1) are conditional upon success of previous time stages.
** Reliability is considered to be an estimated value throughout this section.

The variable characteristics and their test detail are shown in Table 10. The values of F_{iv} are determined by theoretical analyses, simulating the intended space environment, and by engineering judgment. The variables tests as they apply to the components for each time stage are shown in Table 11.

Let R_{Vij} be the reliability for component j in time stage i considering variables characteristics. R_{Vij} is, then, the product of the reliabilities for the applicable independent variable characteristics for the given component and the stage as computed by equation (33).

Testing by attributes.—Consider the component j where the attribute characteristic a is tested. Suppose the characteristic is tested in a specimen size s_a by a random sample of size N_a resulting in c_{ia} failures considering time stage i. The fraction of failure x'_{ia} for a specimen size s_a can be estimated by the expression

$$x_{ia} = \frac{c_{ia}}{N_a} \tag{34}$$

Consider component j to be of size S_j. There are, then, S_j/s_a specimens in component j. The estimated number of failures for component j in stage i when subjected to the test conditions measuring characteristic a is $\left(S_j/s_a\right) x_{ia}$. But in operation only a fraction P_{ia} of this number will be subject to the conditions present in the attribute test a. The estimated number of failures, then, for component j in stage i by characteristic a is $\left(S_j/s_a\right)\left(x_{ia}\right)\left(p_{ia}\right)$. Again, assuming that the number of failures follows a Poisson distribution, the resulting reliability for component j in time stage i considering characteristic a is

$$AR_{ija} = \exp - \left(S_j/s_v\right)\left(x_{ia}\right)\left(p_{ia}\right) . \tag{35}$$

The attribute characteristics and their test detail are shown in Table 12. The criteria of failure and the fractions p_{ia} are engineering estimates; these are further explained in the summary. The attribute tests as they apply to the components for each time stage are shown in Table 13.

Let R_{Aij} be the reliability for component j in time stage i considering attributes characteristics. R_{Aij} is, then, the product of the reliabilities for the applicable independent attributes characteristics for the given component and the stage as computed by equation (35),

TABLE 10.- VARIABLE CHARACTERISTICS AND TEST DETAIL

Characteristic	v	Test	Units of Measurement	s_v	F_{1v}	F_{2v}	F_{3v}
Static material strength	1	Tensile strength	dyn/cm^2	51.6 cm^2	68.95×10^6	48.27×10^6	---
Dynamic material strength	2	Tensile impact	dyn-cm	19.3 cm^2	0.007	0.004	---
Seal Strength following thermal shock	3	Thermal shock	dyn/cm^2	2.54 cm	68.95×10^6	48.27×10^6	---
Seal strength following thermal flexure	4	Thermal flexure	dyn/cm^2	2.54 cm	68.95×10^6	48.27×10^6	---
Seal strength in creep	5	Seam creep	mm	2.54 cm	1.02*	1.52	---
Material reflectance	6	Reflectance	%	0.907 cm^2	---	---	73%

*Indicates maximum successlevel (all others are minimum).

TABLE 11.

Component Variables Tests

Component	j	S_j	Stage	v i = 1	v i = 2	v i = 3
Gore	1	2918.5 m^2	1	1	6	
			2	2	--	
Seal	2	3908.1 m	3	3	--	
			4	4	--	
			5	5	--	
Outer pole cap	3	1.48 m^2	1	1	6	
			2	2	--	
Inner pole cap	4	1.48 m^2	1	1	--	
			2	2	--	
Outer cap seal	5	6.1 m	3	3	--	
			4	4	--	
			5	5	--	
Inner cap seal	6	6.1 m	3	3	--	
			4	4	--	
			5	5	--	
Final seal	7	46.9 m	3	3	--	
			4	4	--	
			5	5	--	

TABLE 12.

Attribute Characteristics and Test Detail

Characteristic	a	Test	s_a	stage	i = 1		i = 2			
				Criteria of failure	P_{1a}		Criteria of failure	P_{2a}	Criteria of failure	P_{3a}
Adhesion in canister	1	Mylar adhesion	644 cm^2	tear	$p_{11} = 1.0 \times 10^{-6}$		tear	$P_{21} = 1.0 \times 10^{-8}$	--	--
Adhesion in manufacturing	2	Hot-wheel Adhesion	361 cm^2	tear	$p_{12} = 1.0 \times 10^{-6}$		tear	$p_{22} = 1.0 \times 10^{-8}$	--	--
Seal strength in peel	3	Seam peel	1.27 cm	<0.58 x 10^5 dyn and no tear	$p_{13} = 1.0 \times 10^{-6}$		<0.58 x 10^5 dyn and no tear	$p_{23} = 1.0 \times 10^{-8}$	--	--
Aluminum flaking	4	Alum.adhesion	29.1 cm^2	--	--		--	--	flake	$p_{34} = 1.0 \times 10^{}$

TABLE 13.

Component Attributes Tests

Component	j	S_j	Stage	a i = 1	a i = 2	a i = 3
Gore	1	2918.5 m^2		1	1	4
				2	2	--
Seal	2	3908.1 m		3	3	--
Outer pole cap	3	1.48 m^2		--	--	4
Inner pole cap	4	1.48 m^2		1	1	--
				2	2	--
Outer cap seal	5	6.1 m		3	3	--
Inner cap seal	6	6.1 m		3	3	--
Final seal	7	46.7		3	3	--

Manufacturing defects.—Manufacturing defects can occur in two major categories of components. These are (m) sphere material and (s) sphere seals. Suppose d_m and d_s defects are located by an inspection function which is E_m and E_s effective for defect location. The estimated number of existing defects D_m in sphere material of area A and defects D_s in sphere seals of length L can be expressed as

$$D_m = \frac{d_m}{E_m} \tag{36}$$

and

$$D_s = \frac{d_s}{E_s} , \tag{37}$$

respectively. There are estimated to be $(D_m - d_m)$ and $(D_s - d_s)$ undetected, unrepaired defects remaining in sphere material and seals, respectively. Suppose P_{im} and P_{is} are estimates of the fraction of unrepaired defects which will cause mission failure in stage i. The estimated numbers of failures caused by undetected, unrepaired material and seal defects are $P_{im}(D_m - d_m)$ and $P_{is}(D_s - d_s)$, respectively. Consider, again, component j which is of size S_j and is of either category (m) or category (s). A proportional estimate of the remaining defects in component j can be expressed as $(S_j/A)(D_m - d_m)$ or $(S_j/L)(D_s - d_s)$ and the estimated number of failures becomes $S_j(P_{im}/A)(D_m - d_m)$ or $S_j(P_{is}/L)(D_s - d_s)$. Following the Poisson distribution, defect reliability for component j in stage i becomes

$$R_{Dij} = \exp - S_j(P_{im}/A)(D_m - d_m) \tag{38}$$

or

$$R_{Dij} = \exp - S_j(P_{is}/L)(D_s - d_s). \tag{39}$$

The estimates P_{im} and P_{is} are determined by historical data from previous spheres. These appear by component and time stage in table 13.

Similarly, the inspection effectiveness can be classified in categories (m) and (s). Material is subject to four independent 100 per cent inspections and seals are subject to three independent 100 per cent inspections. The effectiveness of inspection E can be estimated by the expression

$$D = 1 - (1 - q)^n , \tag{40}$$

where q is the fraction effective of a single 100 per cent inspection and

n is the number of 100 per cent inspections. The fraction effective q is taken to be .87 based on previous inspection experience and studies conducted in statistical quality control. The effectiveness, then, for category (m) is $E_m = 1 - (1 - .87)^4 = .99971$ and for category (s) is $E_m = 1 - (1 - .87)^3 = .99780$. Inspection effectiveness by component is also shown in Table 14.

Defect reliability by component can be computed by the general equation (38) or (39).

Component reliability prediction.—Expressions have been now developed for estimating the reliability of each component in each time stage considering variables testing, attributes testing, and manufacturing defects. The resulting independent reliabilities are R_{Vij}, R_{Aij}, and R_{Dij}. Expressing these in terms of the reliability for component j in time stage i, we obtain

$$R_{ij} = R_{Vij} \cdot R_{Aij} \cdot R_{Dij} \tag{41}$$

The above expression can be used to develop component reliability prediction expressions by time stage.

Equation (41) solves for the reliability of each applicable component j in each time stage i with the exception of the inflatants (j = 8) in time stage i = 1. No tests by either variables or attributes are available for this component. There is no known method in which defects can be evaluated in terms of an estimated number of failures. However, based on success of Echo I and II, and theoretical computations and verification of the PAGEOS inflation system, the reliability prediction of the inflatants is set as $R_{18} = .9996$.

The reliability of each applicable component j in each time stage i has now been estimated. Following the exponential distribution, each such reliability can be expressed as

$$R_{ij} = \exp - (k_j \lambda_{ij} t_i) \tag{42}$$

or using the Poisson distribution for the case of cycles

$$R_{ij} = \exp - (k_j \lambda_{ij} C_i) \tag{43}$$

where k_j is the quantity of component j in the system, λ_{ij} is the failure rate per unit time (or per unit cycle) of the j^{th} component in stage i, t_i is the operating time in stage i, and C_i is the number of operating cycles in stage i. Table 15 identifies quantities of k_j for the respective components in a single Inflatable Sphere Assembly.

TABLE 14.

Defect Fractions of Failure and Inspection Effectiveness

Component	j	stage i = 1	i = 2	i = 3	E_m or E_s
Gore	1	P_{1m} = .56000	P_{2m} = .56000	P_{3m} = .16000	E_m = .99971
Seal	2	P_{1s} = .04065	P_{2s} = .02439	---	E_s = .99780
Outer pole cap	3	P_{1m} = .56000	P_{2m} = .56000	P_{3m} = .16000	E_m = .99971
Inner pole cap	4	P_{1m} = .56000	P_{2m} = .56000	---	E_m = .99971
Outer cap seal	5	P_{1s} = .04065	P_{2s} = .02439	---	E_s = .99780
Inner cap seal	6	P_{1s} = .04065	P_{2s} = .02439	---	E_s = .99780
Final seal	7	P_{1s} = .04065	P_{2s} = .02439	---	E_s = .99780

For time stage i = 1, equation 43 can be used to compute component failure rates, λ_{1j}, for j = 1, 2, •••, 8 since R_{1j} is known* and C_1 = one cycle. Equation 42 applies likewise for computing failure rates of components j = 1, 2, •••, 7 in time stage i = 2 where R_{2j} is known* and t_2 = 336 hours. For components j = 1 and 3, failure rates in stage i = 3 can be determined by equation 42, as R_{3j} is known* and t_3 = 43,800 hours.

TABLE 15:- COMPONENT QUANTITIES

Component	j	k_j
Gore	1	84
Seal	2	83
Outer pole cap	3	2
Inner pole cap	4	2
Outer cap seal	5	2
Inner cap seal	6	2
Final seal	7	1
Inflatants	8	1

Time stage and system reliability prediction.—Having predicted reliability by component and found component failure rates, it becomes necessary to examine time stage reliability leading to a reliability prediction of the system. Time stage reliability can be expressed as

$$R_i = \exp - (\lambda_i t_i) \text{ for stages } i = 2 \text{ and } 3 \qquad (44)$$

and

$$R_i = \exp - (\lambda_i C_i) \text{ for stage } i = 1 \qquad (45)$$

shere λ_i is the failure rate for the system in time stage i.

The stage reliability, R_1, is the product of the applicable component reliabilities, R_{ij}, in the time stage i. After solving for R_1, R_2, and R_3; λ_i for stages i = 1, 2, and 3 can be solved by equations (13) or (14).

* The values of R_{ij} are computed from equation (41).

The reliability prediction for the Inflatable Sphere Assembly, then can be determined by the expression

$$R_{system} = R_1 \cdot R_2 \cdot R_3 \tag{46}$$

Substituting equations (44) for stages 2 and 3 and 45 for stage i = 1 into equation (46) we obtain

$$R_{system} = \exp - (\lambda_1 C_1 + \lambda_2 t_2 + \lambda_3 t_3) \tag{47}$$

where the values of C_1, t_2, and t_3 are known.

Summary.—In the preceding paragraphs, a mathematical technique for a reliability prediction model for PAGEOS Inflatable Sphere Assemblies has been developed. The model is built considering several established premises and engineering judgments. These are further defined as follows:

Randomness of samples: The validity of the statistical estimates are based upon the premise that the test specimens are drawn at random.

Establishment of failure levels: Failure levels for test results are determined through evaluation of historical sphere data and theoretical analyses.

Reliability distributions: In the case of components where the number of failures is of concern, and also in the case of survival of cycles, the Poisson distribution is assumed to hold. Wherever survival time is of concern, the exponential distribution (with a constant failure rate) is assumed to hold. In all cases, reliability is the estimate of the probability of survival (occurrence of no failures).

Normality: The premise of normality is applicable to all variables tests with the exception of that of tensile impact (v = 2). Normality tests support this premise and show that the probability distribution for tensile impact is considerably skewed to the right. If estimates considering tensile impact were based on normality, the fractions of failure would be unjustly high, resulting in an underestimate of reliability. The test of normality suggests that the left half of the distribution ($-\infty$ to μ_2) is normal*. Since only the lower level of failure for the distribution is of concern, the sample mean and standard deviation can be graphically determined on probability paper using only the left half of the plotted cumulative probabilities. Once these estimates are established, the estimated number of failures can be determined in the same manner as for other variable tests.

Test validity and expectations of failure: The mathematical development is based on the premise that the tests measure critical characteristics and that each test result is a representative measurement of its associated characteristic.

For variables testing a single test specimen which reaches a failure

*The mean μ_2 is also considered to be the median.

level is considered to be cause for component failure in the respective time stage and will result in mission failure.

For attributes testing, it is recognized that the component will be directly subject to the conditions of the tests only a very small percentage of the time. Consider the four attributes tests as follows:

1. PET adhesion. The purpose of this test is to simulate canister blocking conditions. However, the test is conducted without inflatants, whereas canister conditions include inflatants which preclude adhesion. The test data measure the potential to fail, where in the canister only a very small portion of the specimens will be subjected to the simulated test conditions. If these conditions (accordion pleats or zigzag folds of material without inflatants under heat and pressure) occur in the canister, the material must also have the potential to adhere and tear for failure to occur.

2. Hot-wheel adhesion. This test simulates the condition of material passing beneath the hot sealing wheel resulting in inclusions and potential adhesion. However, since many precautions have been taken to preclude this, only a very small fraction of material, if any, will be subject to this condition. The test results measure the potential to adhere. However, in order to be cause for failure, the material must be subjected to hot-wheel adhesion conditions, must have the potential to adhere and tear, and this condition must be undisclosed by inspection.

3. Seam peel. Seam peel is not a normal condition in any of the three time stages of operation. Failure will result only if the seal is subject to peel and also has the potential to fail in peel. The test measures the potential to fail. The seal, however, will be subjected to tensile conditions which are measured through the seal variables tests. In addition, the adequacy of the back-up sealing wheel was evaluated under separate study. Tensile strength after thermal shock was tested over the entire circumference of the wheel, and no tensile failures occurred within the seam.

4. Aluminum adhesion. Again, the test conditions are only remotely probable during the operation time stages. Metalizing defects, however, can be induced by handling during fabrication. These conditions are evaluated by the manufacturing defect portion of the model.

Manufacturing defect evaluation: The fabrication defect evaluation development of the model is based on the premise that if a defect is located, it is repaired satisfactorily and the repair will result in performance comparable to a defect-free component. Therefore, failure can occur only in the case where defects are not located by inspection.

Relevant data and independence: The characteristics measured by both variables and attributes testing are considered to be independent, and tests are assumed to measure the entirety of characteristics which have the potential to cause failure.

Homogeneity of components: Each component is considered to be of the same general structure throughout its entire size (area or length).

Adhesion during inflation: The mode of failure during inflation is considered to be material tearing caused by adhesion. If adhesion occurs, the folds are assumed to either open or the material will tear.

Reliability predictions by components and stages for Inflatable Sphere Assemblies 2, 3, and 4 are shown in Figures 20, 21, and 22, respectively.

FABRICATION

Material Treating and Inspection

The material treating operation was the first step in processing the aluminized PET. Its purpose was to prevent the PET side of the material from adhering to itself during the fabrication processes, and during the storage of the sphere prior to its deployment in space. The process consisted of coating a solution of Freon TF and cationic detergent on the PET side of the aluminized material, and passing it through a drying tunnel where the solvents were evaporated. The relative web speed past the reverse coating roller was about 12 m/min. Room temperature conditions were maintained in the coating bath and first stage drying tunnel. The second stage tunnel was operated at 54.4 C. Figure 23 shows the web threading diagram of the treating machine.

The aluminized PET was then visually inspected to detect, identify and flag any material defects. The aluminized side of the material was inspected for pinholes, pinwindows, and other defects by passing it between a light source and an inspector in a darkened area. (See figure 24.) The light was diffused by a simple translucent plastic shield and was located 5 cm from the web to produce optimum inspection conditions. The illumination at the PET was 1076 lumens/cm^2. It then passed outside the darkened area to normal lighting conditions and was inspected on the PET side by a second operator. During the inspection, material was cut into 51.8-m gore blanks and material acceptance test samples were cut and sent to the Material Testing Laboratory. Table 16 summarizes the defects and the possible corrections.

Gore Cutting

The next step in the manufacturing sequence was to tailor the gore blanks into sections which, when sealed together, would form a 30.48-m diameter sphere. The material was dispensed on a long flat table fitted with guide rails (gore template) which formed the outline of the gore. The gores were cut by blades which followed the guide rails on the table. Increment marks were made along both gore edges every 30.5 cm to facilitate alinement during the sealing operation. A 2.54-cm diameter tape disc was sealed near one gore edge at the

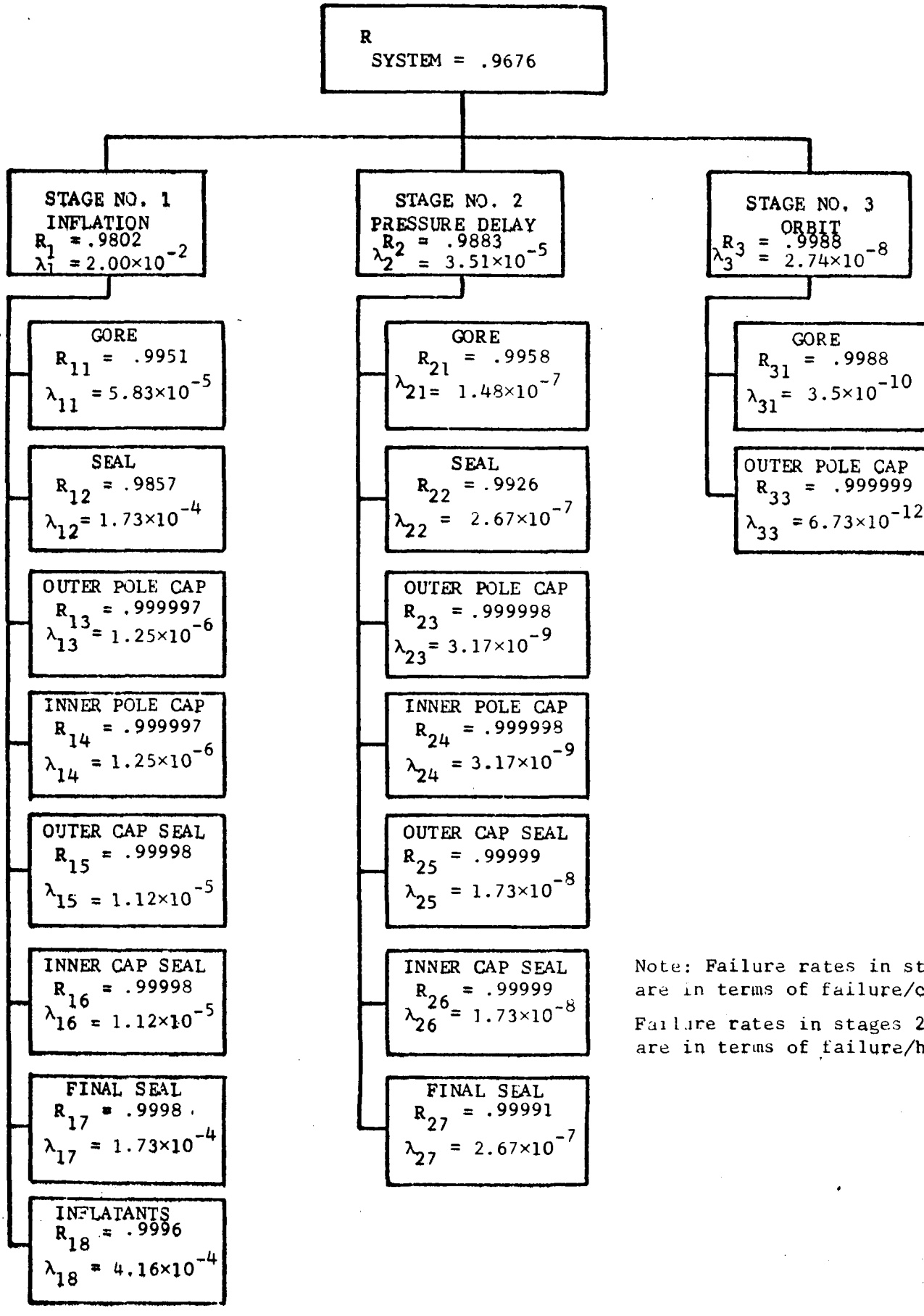

Note: Failure rates in stage are in terms of failure/cycle

Failure rates in stages 2 and are in terms of failure/hr.

Figure 20.- Sphere No. 2 Reliability block diagram.

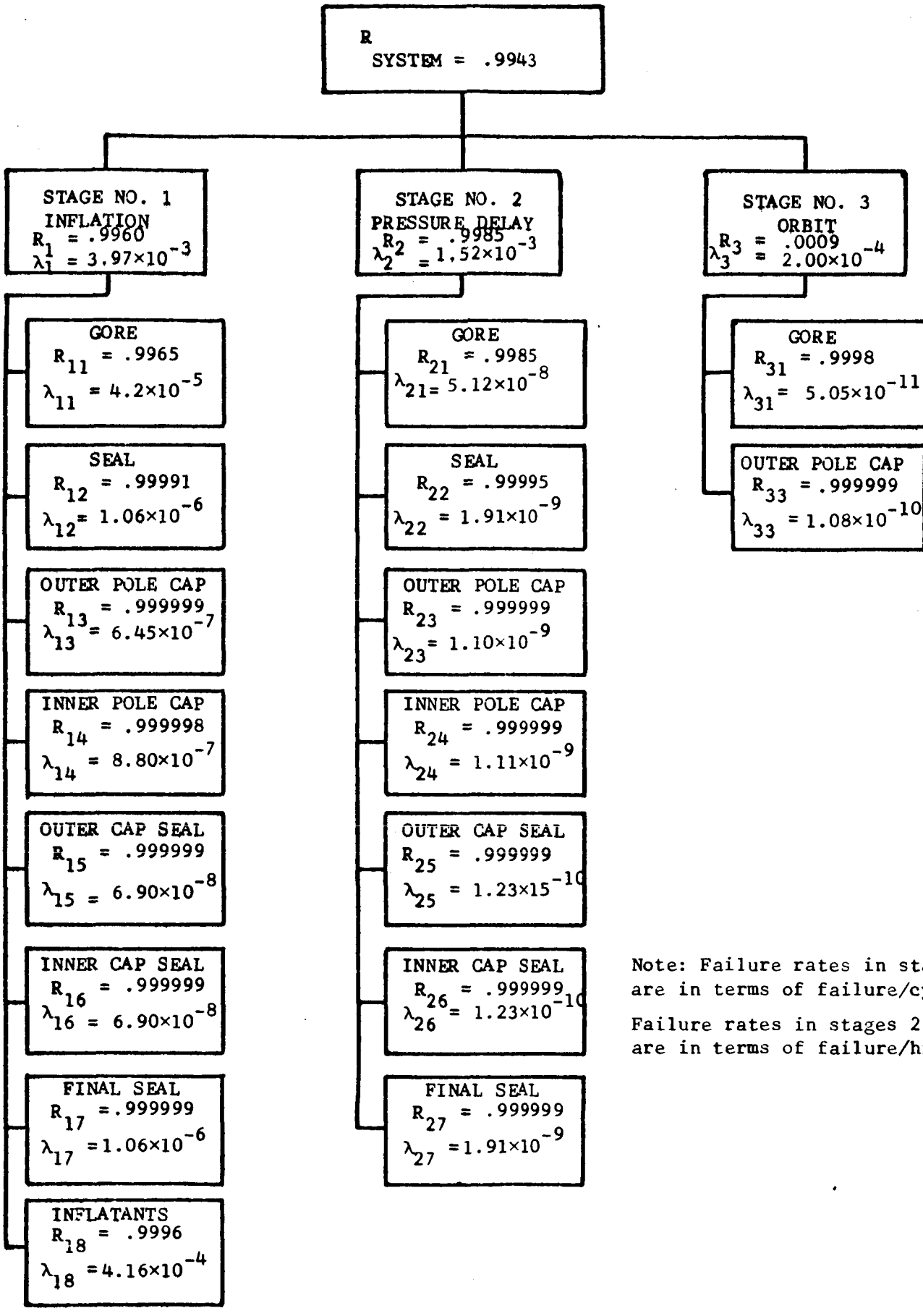

Note: Failure rates in stage 1 are in terms of failure/cycle.

Failure rates in stages 2 and 3 are in terms of failure/hr.

Figure 21.- Sphere No. 3 Reliability block diagram.

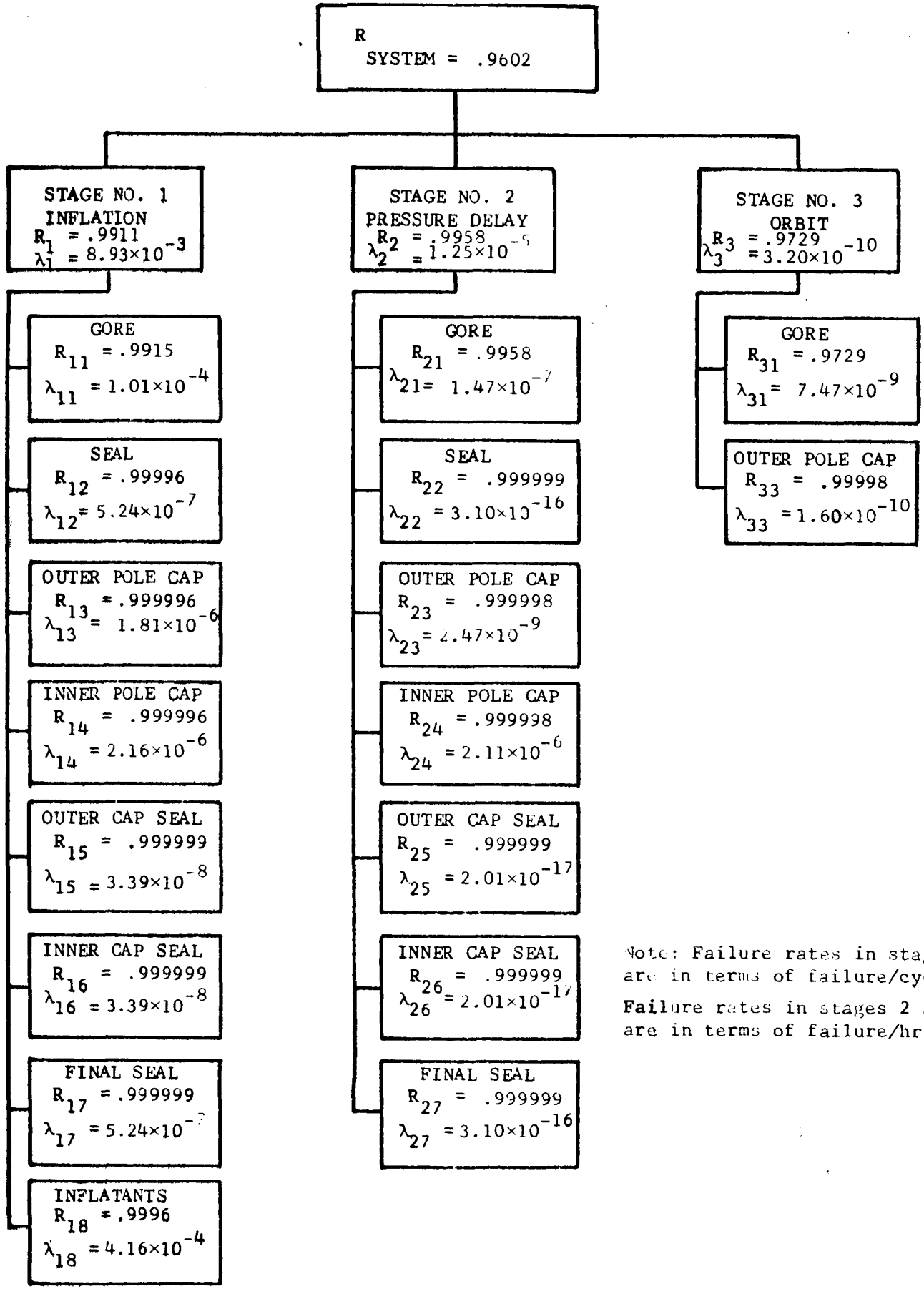

Note: Failure rates in stage 1 are in terms of failure/cycle.

Failure rates in stages 2 and 3 are in terms of failure/hr.

Figure 22.- Sphere No. 4 Reliability block diagram.

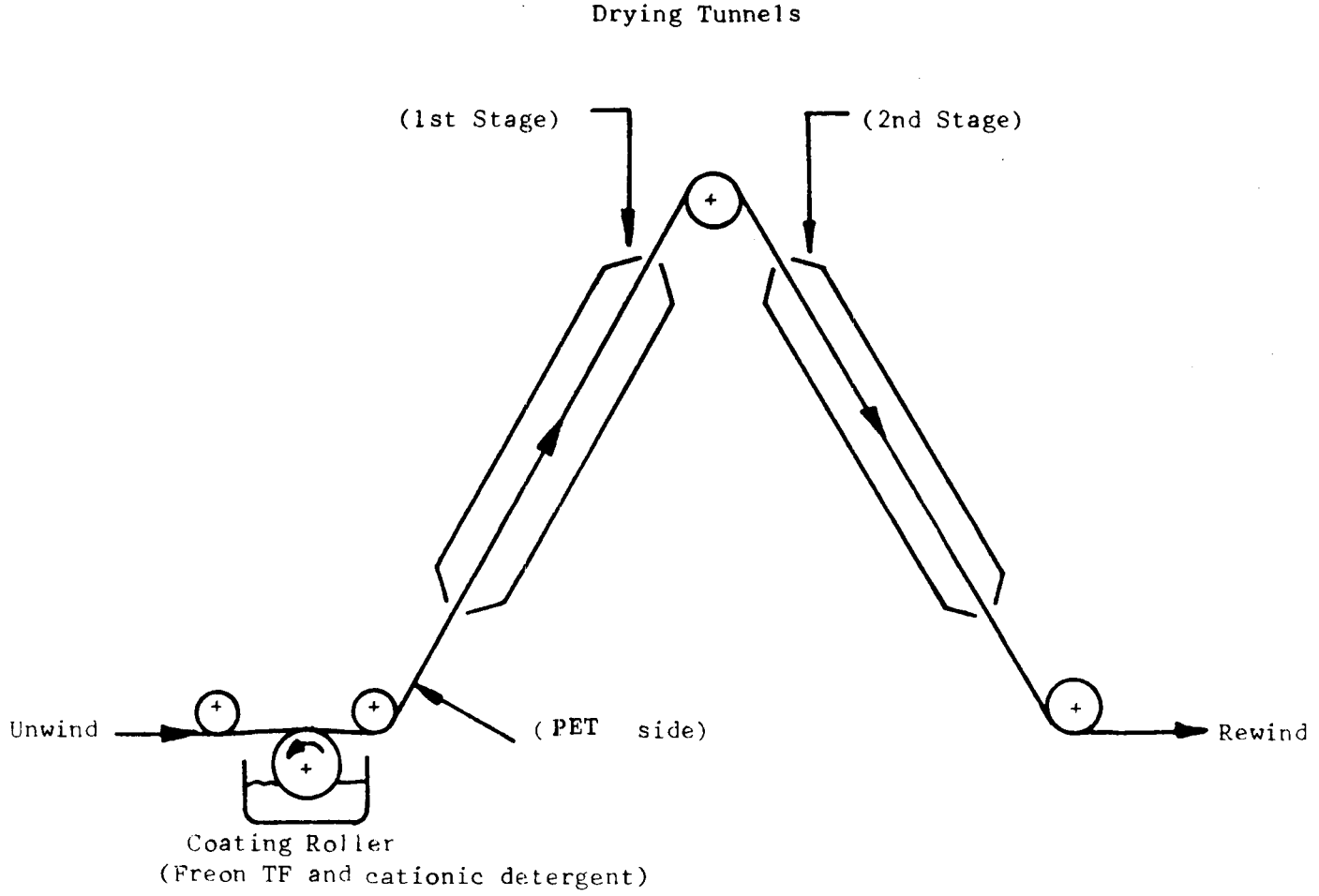

Figure 23. - Web threading diagram of treatment machine.

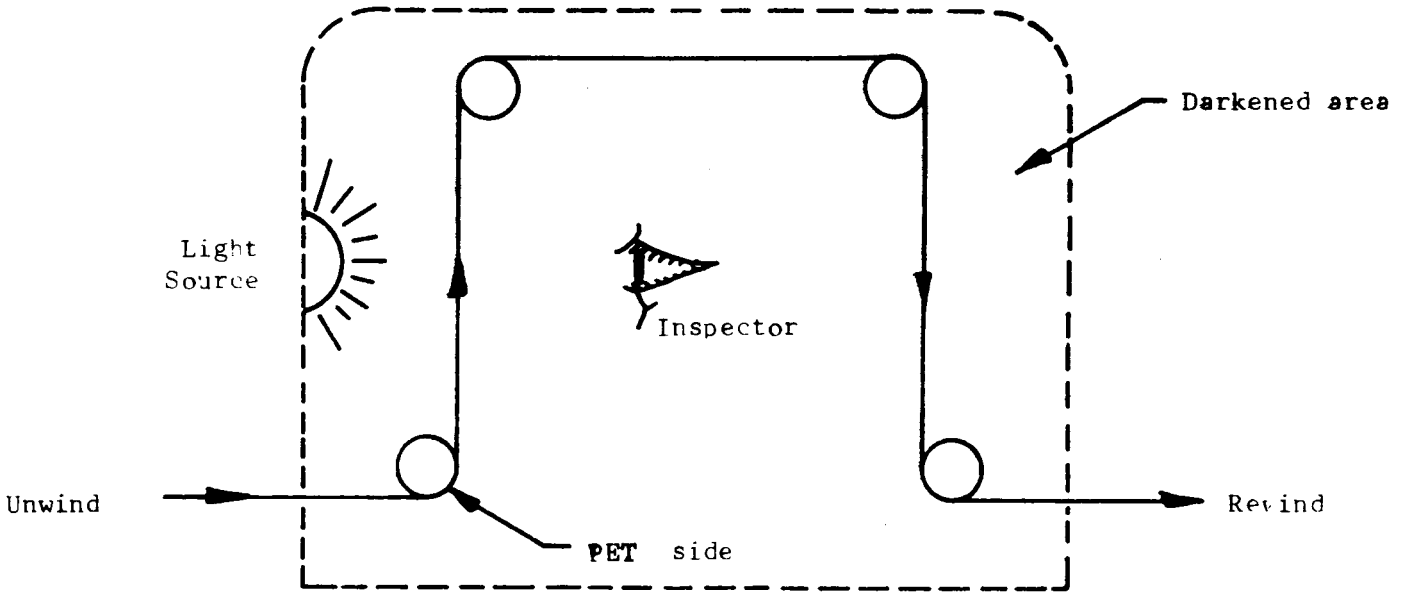

Figure 24. - Web threading diagram of inspection machine.

TABLE 16.- CLASSIFICATION OF DEFECTS

Materials Tests	Reject	Repair
Tensile strength	Less than 1241 x 10^6 dyn/cm^2	None
Tensile impact	Less than 4.2 × 10^6 dyn-cm	None
Reflectance & specularity	Less than 83% reflectance or greater than 90%	None
Aluminum adhesion	Aluminum on tape	None
Gore weight	Exceeds range 626 ± 64 gms	None
Thickness	Exceeds ± 10% nominal thickness	None
1 ohm per square	More than 1 ohm per square	None
Sealing-wheel adhesion	Tear in sample	None
Canister-simulation and adhesion	Tear in sample	None
Tape age	Over 30 days	None

TABLE 16.- CLASSIFICATION OF DEFECTS (Concluded)

Seam Tests	Repair	Gore Removal
Flexure	Failure: Use bitape and requal. Use 0.85 cm dia. dowel.	Requalifying action fails
Thermal shock	Failure: bitape and requal.	Requalifying action fails
Seam creep	Exceeds 0.5 mm at 150 C and 138×10^6 dyn/cm^2. Add bitape.	
Seam peel	See note (f). Failure: Add bitape and requalify.	Requalification value plus original value less than 0.58×10^6 dyn
Seam half width	Less than 1.02 cm for 2.54 cm wide and less than 0.64 cm for 1.91 cm wide.	
Seam gap	Exceeds 7.6 mm	See notes
Seam overlap	Exceeds 1.27 mm	See notes
Miscellaneous		
Alinement marks	Exceeds 0.152 cm	See notes
Foldover	Greater than 0.16 cm and within the tape	Outside the tape
Patches		
Patches (gores)		Exceeds 348.4 cm^2 per gore

Notes - Seal Repair Limitations

(a) Maximum single repair length per seal shall not exceed 2.4 meters.
(b) Maximum total repair length per seal (excluding gore replacement) shall be 4.57 meters.
(c) Repair cut to be 30% longer than the defect length on either side.
(d) Splice plate repair tape shall extend a minimum of 5.08 cm beyond the cut length on either side of the out-of-tolerance length.
(e) All repair cuts to be peel tested and combined values shall be greater than 0.58×10^6 dyn. Failure requires gore removal.
(f) Failure of the first peel test plus failure of either the first flexure test or the first thermal shock test shall require gore removal.

equator for alinement reference during the powdering operation. The cut gore was rewound on a core, weighed, and wrapped for storage. Figure 25 shows the cutting operation.

Gore Sealing and Assembly

Prior to sealing the gores, they were balanced according to a specified weight tolerance, and assigned to various positions in the sphere. Individual gores were required to weigh 626 $\pm$ 64 gms. To balance the gores, those four gores assigned positions 90 degrees apart were required to weigh within 14 gms of each other. The gores were joined at the edges, one at a time. The gore edges were cleaned with solvent before sealing to insure a reliable bond, and the seal cleaned on both sides after sealing to remove any traces of residual adhesive. Sealed gores were draped over the sealing table center rail where they were exposed for inspection. (See figure 26.)

During the assembly of the PAGEOS spheres a number of subassembly operations were conducted. These operations were as follows: vent hole assembly, part final seal, polar cap installation, continuity ring installation, inflatant installation, and the final seal.

Vent holes.—The vent holes are 0.16-cm diameter holes placed in the two gores which are on the outside of the pleated stack of the sphere. These gores are 180 degrees apart in the inflated sphere. One hole was located at each zigzag; their purpose was to bleed air from the sphere after it was packaged into the canister.

Polar cap and part-final seal.—The polar caps and part-final seals were installed on the sphere after the gores were sealed together. The part-final seal was approximately 0.9-m long, and was made at the tips of the sphere so that the unsealed edges of the first gore and the last gore of the balloon were joined together. The purpose of installing the part-final seal was to permit end cap installation before the final seal was made.

The polar cap assembly consisted of two pieces, an inner and an outer cap (see figure 2). The inner cap was made from 0.0254-mm clear PET and was the structural member of the polar cap. The outer cap was made from 0.0127-mm metalized PET, contained vent holes, and was the ultraviolet shield for the polar cap assembly.

Continuity ring.— After the polar caps had been installed, two continuity rings were installed, an inner and an outer ring. Both rings were on the outside, aluminized side, of the sphere. The inner ring connected the polar cap with the ends of the gores, and consisted of a silver conductive paint applied around the edges of the outer polar cap. The purpose of this ring was to provide dc continuity between the gores and the outer polar cap. A metalized PET tape ring was then installed over the painted area to protect the silver paint from abrasion during folding and packing. After this ring was installed, an electrical continuity check was made. The outer continuity strip was similar in design and purpose to the inner continuity strip, but

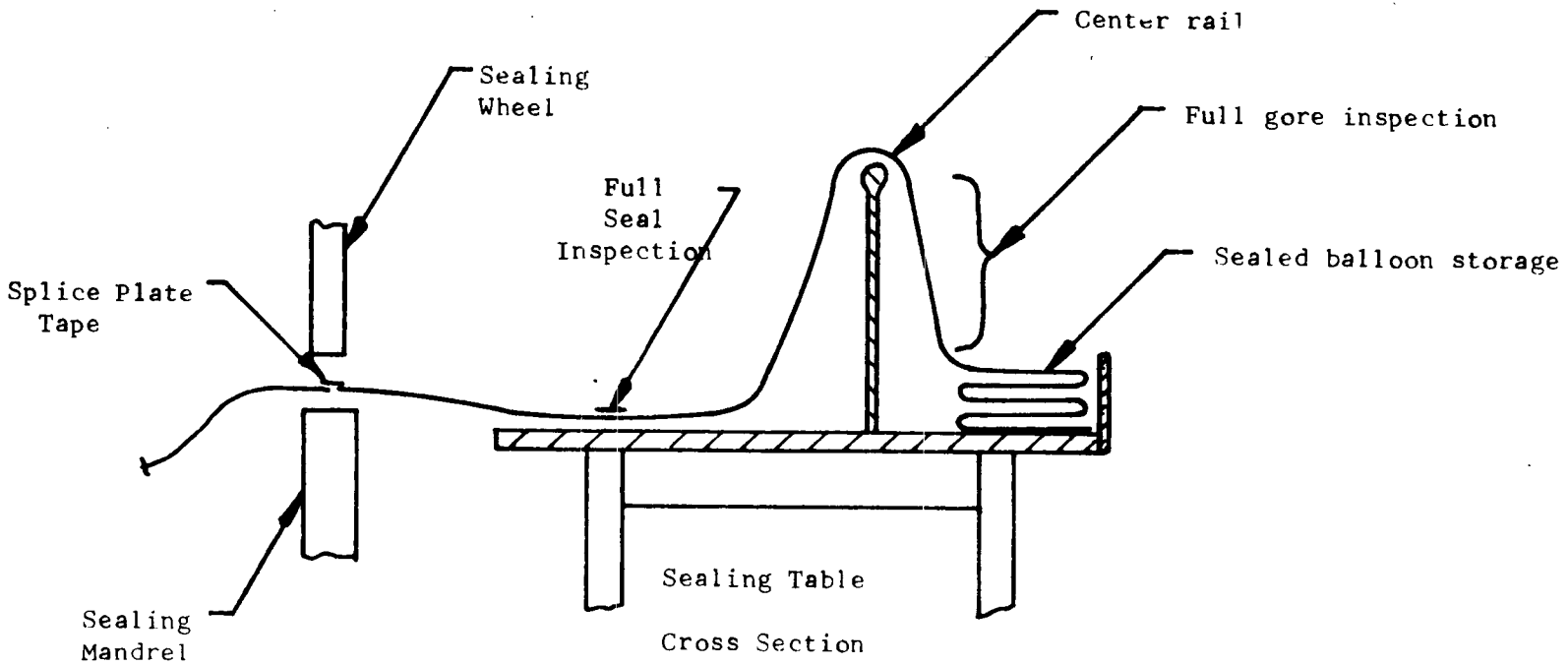

Figure 26 - Gore sealing diagram.

was 7.6 cm farther out from the polar cap, and connected the gores to one another. This continuity strip consisted of the silver paint and a 0.3-cm aluminum laminate bonded to the gores. Thermosetting tape was also bonded over this continuity strip for protection.

Final seal.—The last special assembly was the final seal. After the sphere had been completed and the inflation system installed, the final seal was used to close the remaining opening in the balloon. The final seal consisted of two tapes coated with thermosetting adhesive, an inner, 1.9-cm wide, clear tape, and an outer 2.54-cm wide aluminized tape.

Inflation Compound Installation and Pleating

After the polar caps and continuity strips had been installed in the sphere, the inflation system was added. This operation was performed in a temperature and humidity controlled atmosphere.

The inflation system consisted of two powdered chemicals dusted between the layers of the sphere as it was being pleated. The inflatant powders were anthraquinone and benzoic acid. These powders, when exposed to the pressure and temperature of space, sublime and change to a gas which inflates and pressurizes the sphere.

The powder distribution was intended to produce controlled inflation as the sphere deployed. To effect this 4.54 Kg of benzoic acid and 2.27 Kg of anthraquinone was dusted in the equatorial half of the sphere area, which was to deploy first; and 6.80 Kg of anthraquinone was dusted over the remaining half of the sphere (polar areas).

Accordion pleating consisted of laying the sphere out, full-length on a shelf, above the pleating and powdering table. The material was then fed down to the pleating table where 5 pleats were put in each gore with the aid of a contoured plastic template. Aliquot parts of inflation powders were dusted into each pleat as it was made except the two adjacent to the final seal. These two were left undusted to leave a clean bonding surface.

The final pleated stack was 45.7 cm wide at the center and tapered to 15.2 cm at each end. This long thin configuration was necessary to produce a folded stack which would fit in a canister as a sphere was zigzag folded in a later operation. Figure 27 shows the various steps of pleating, folding, and packing the sphere.

Canister Packing

Following the final seal operation the sphere was placed in a plastic sleeve which was evacuated to remove excess air from the sphere and to "set" the pleats prior to the canister packing operation. Prior to packing, air wicks were placed in both halves of the canister to help bleed air from the balloon during the evacuation process. In the packing operation half of the sphere was packed into each canister half as shown in steps 2 and 3 of Figure 27.

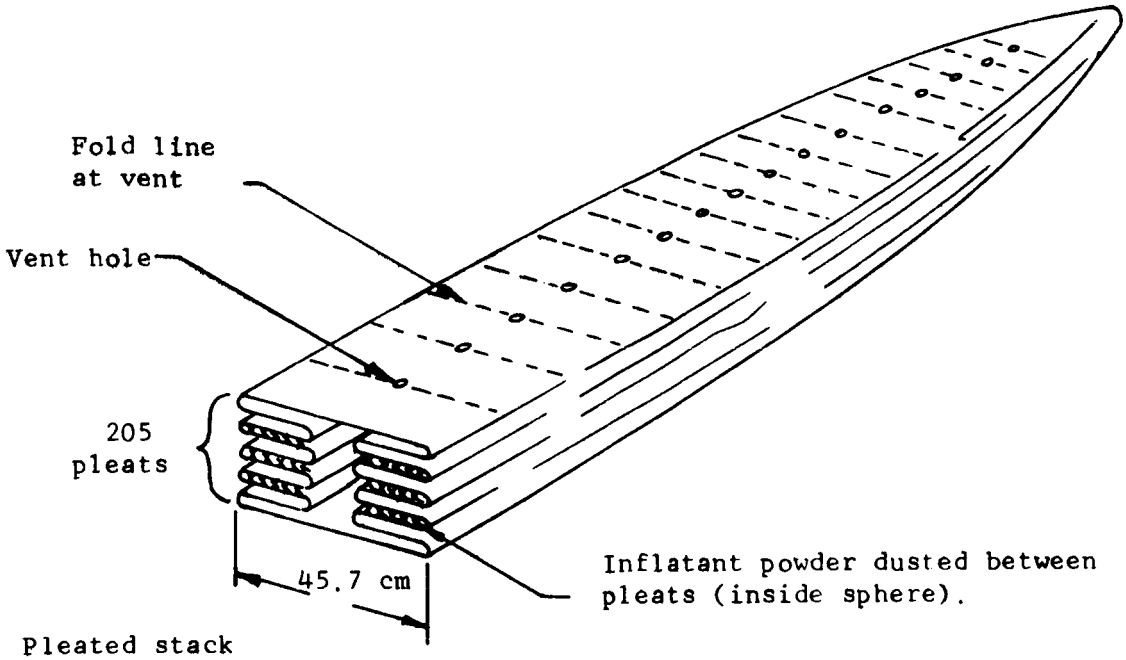

Step 1

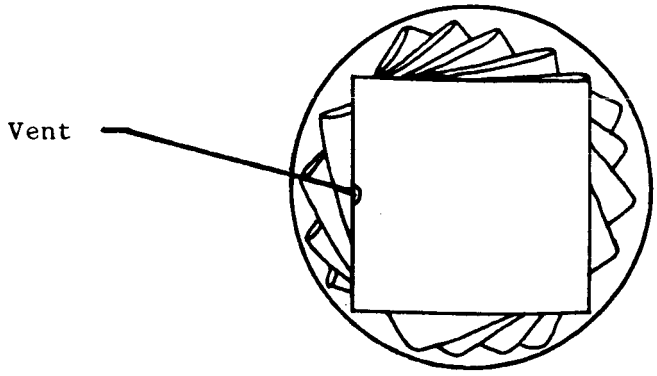

Top view of lower canister half.
(Rotation of sphere during zigzag folding)

Step 2

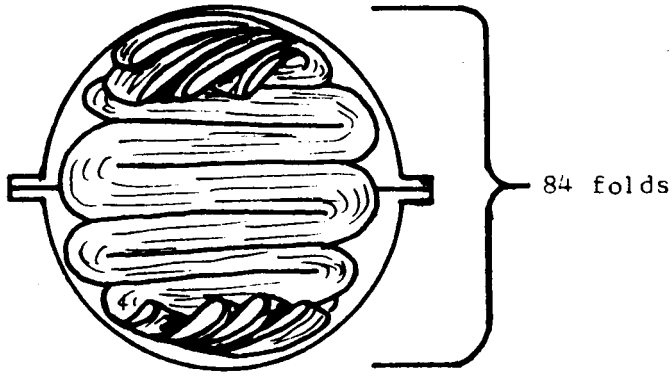

Side view of pleated, rotated, and folded
sphere in spherical canister.

Step 3

Figure 27.- Folding and packing.

After the two canister halves had been packed, the top canister half was lifted and placed on the lower half. Prior to closing, smoke shields were placed inside the canister flanges to protect the balloon from pyrotechnics (used during canister separation) entering this area. The canister was then ready for the closing operation.

Canister Evacuation and Weight Determination

The evacuation process removed the air from the canister and from within the balloon. The slightly open canister was placed in a vacuum chamber equipped with closing wrenches. The air was then removed from the vacuum chamber slowly to prevent excess differential pressure from building up within the balloon. The vacuum chamber pressure was regulated to maintain a pressure of less than 133.3 dyn/cm^2 for 72 hours to permit outgassing of the sphere. A 12 hour check with the chamber sealed off was then made to determine completeness of evacuation. Following removal of the air the canister was closed inside the vacuum system. After closing was complete, the sealed canister was exposed to atmospheric pressure and checked for leakage prior to shipment. After the leakage check, the canister was packed in a shipping container where temperature and pressure in the canister were recorded automatically until the final use of the packaged satellite.

The last step in the evacuation process was determining the weight of the packaged sphere. The canister, and components added during the packing stage, were weighed prior to packing of the sphere, since the sphere could not be weighed separately. After evacuation, the packed canister was again weighed to obtain weight loss due to evacuation. The difference yielded the sphere weight.

The following Table 18 gives the weights, identification, and disposition of each of the spheres.

Sphere Handling

During the manufacture of the inflatable sphere assembly, a number of handling precautions were taken. These precautions aided in retaining the original material properties, and prevented possible damage or contamination from affecting the completed space craft. The precautions taken were as follows:

1. Relative humidity was maintained below 50 per cent to keep inflation system dry during installation.

2. Temperature was controlled to 22 $\pm$ 3 degrees C to provide optimum conditions for sealing operations and inflation systems installations.

3. Work tables and equipment were covered with soft plastic to protect sphere materials from abrasion and puncture damage.

TABLE 18.- SPHERE DESCRIPTIONS AND DISPOSITIONS

SPHERE NUMBER	DESCRIPTION	WEIGHT (Kgs) POWDER	PREEVACUATION	POSTEVACUATION	DISPOSITION
1	Static Inflation Test	*	67.218	*	Destruction Tested
2	Prototype	13.791	67.558	66.706	Vacuum deployment Test (Langley Research Center)
3	Prime	13.852	67.229	66.974	Flight Backup (Langley Research Center)
4	Standby	13.656	68.104	67.941	Orbited June 23, 1966
5	Backup	*	54.659	*	Spare, shipped to Langley Research Center
6	Backup	*	53.978	*	Spare, shipped to Langley Research Center

*These spheres did not have inflation powder and were not packed in canisters.

4. Gloves were worn by personnel touching sphere to protect the metalized surface from finger prints and body oils.

5. Smoking or eating was not permitted in fabrication area to prevent contamination of the sphere.

6. Sharp hand tools and measuring instruments were not permitted to be used on sphere to protect it from punctures.

7. Hand sealing iron use was carefully controlled and supervised to protect the sphere from shrinkage and burn damage.

8. Access to manufacturing area was controlled to protect the sphere from accidental damage by persons unfamiliar with the material.

9. Shields and fences were placed on certain equipment to protect the sphere from accidental damage caused by operators working on or walking past sphere.

10. Tooling in contact with material was designed with smooth radiused surfaces and corners to protect material from being stretched or punctured.

11. Tables and floors were cleaned frequently to prevent any dust from contaminating the sphere material.

CONCLUDING REMARKS

The stress analysis of the orbital satellite showed that only 8.274 x 10^6 dyn/cm^2 skin stress is necessary to make it spherical when pressurized. However, to maintain a spherical shape without internal pressure a skin stress of 545 x 10^6 dyn/cm^2 is required to yield the material permanently. These calculations are based on room temperature conditions.

The thermal analysis of the orbital sphere when between the sun and earth showed that the expected mean temperature is about 120 C and deviates from this by less than 10 C.

The inflation system selected consisted of two organic chemicals in powder form. It was determined that 4.536 Kg of benzoic acid and 9.072 Kg of anthraquinone were sufficient to inflate and pressurize the 30.48 meter diameter sphere to 79.2 dyn/cm^2. This pressure produced a skin stress of 48.27 x 10^6 dyn/cm^2. The pressure calculations for the anthraquinone were based on the cold spot temperature (102.9 C) of the sphere, since its vapor pressure within the sphere would be controlled by the condensation taking place at that point. The pressure calculations for the benzoic acid were based on the mean temperature (108.5 C) since this vapor would be in contact with all portions of the sphere.

The stress analysis of the static inflation sphere attachments has shown that a safety factor in excess of twice the basic material (0.0127-mm PET) was used in the design.

Advance testing of special attachments necessary for the static test of the 30.48 meter sphere demonstrated that ample safety factors were used in the design of these components. The tie-down patch reached a maximum test rupture loading of 191×10^6 dyn compared to 21.6×10^5 dyn maximum expected for operation. Spherical segments containing duct modifications exceeded 1103×10^6 dyn/cm^2 skin stress without sign of degradation in adjunction areas. Ultimate rupture occurred in areas beyond the modifications indicating that the designs were satisfactory.

The static test of the sphere showed that dimensional requirements of $\pm$ 1/2 per cent of the diameter in both polar and equatorial dimensions were met. The ultimate skin stress at the time of rupture was 689.5×10^6 dyn/cm^2. No seam creep was detected during or after the test. Dc resistance measurements varied between 1 and 200 ohms during the test. After the test the resistance values were higher, between 50 and 300 ohms. The general appearance at stresses above 137.9×10^6 dyn/cm^2, with one exception near the north polar cap, showed the sphere to be an excellent optical reflector. The sphere was very smooth and symmetrical. The point of origin of the rupture is believed to have been a tuck or underlap of the gore material in a seam near the north polar cap.

It was found that under certain conditions of temperature and pressure, the PET side of the aluminized PET would adhere to itself and form a bond. When these bonds were separated the material tore. A chemical treatment process was found which prevented these adhesions. The treatment consisted of coating the PET side of the aluminized PET with a solution of 53 parts per million of cationic detergent in Freon TF. Comparison tests of treated and nontreated PET show no significant degradation of the treated material, except a slight increase in seam creep properties. Thereafter, the PET side of the aluminized PET was chemically treated to prevent adhesions. The total surface area was inspected to detect and identify minute imperfections in the aluminizing and the PET. Representative samples, taken from each gore blank,were tested prior to acceptance of the material.

Special tooling for many operations facilitated accurate fabrication and handling the fragile material. A treating machine was built for chemical treatment of the aluminized PET. An inspection machine, incorporating evaluation of excess light transmission, was built to detect holes in the aluminizing and the PET material. A table containing the gore outline was built for accurate gore cutting and a long, narrow table was built to dispense and control the material during pleating and powdering. A system incorporating inclined ramps and movable carts was developed to package the sphere.

Each phase of manufacturing was covered by one or more kinds of inspection to insure conformance to the specifications and freedom from defects. Special handling techniques were developed during the program to minimize degradation of the aluminized PET and to permit optimum inspection.

ERRATA

PASSIVE GEODETIC SATELLITE

INFLATABLE SPHERE ASSEMBLIES

By S. J. Stenlund, C. A. Dahlgren, A. J. Wendt,
D. Lingo, D. Roiseland, and T. J. Neuhaus

December 1966

Page 2: Add to definitions
20. SIT - static inflation test

Page 5: Figure 1 Capitalize PET

Page 28: Line 5 and in footnote replace blocking with adhesion

Page 39: First two words last paragraph replace a voltmeter with an ohmeter

Page 41: Seam peel acceptance criteria replace 0.0232 Kg/cm with 0.0228×10^6 dyn/cm

Page 45: Table 6 First item replace canister simulation with PET
Second item replace Sealing-Wheel with Hot-Wheel

Page 65: Table 10 Last item replace material with aluminum

Page 67: Table 12 First item replace Mylar with PET

Page 74: First word 7th line replace blocking with adhesion

Page 81: Eighth item replace sealing-wheel with hot-wheel
Ninth item replace canister simulation and with PET

Issue date Jan. 16, 1967